The plant cytoskeleton, NET3C and VAP27 mediates the link between the plasma membrane and endoplasmic reticulum

Pengwei Wang[1], Timothy J. Hawkins[1], Christine Richardson[1], Ian Cummins[1], Michael J. Deeks[1#], Imogen Sparkes[2#], Chris Hawes[2] and Patrick J. Hussey[1*]

[1] School of Biological and Biomedical Sciences, University of Durham, South Road, Durham, DH1 3LE, UK

[2] Department of Biological and Medical Sciences, Oxford Brookes University, Gipsy Lane, Headington, Oxford, OX3 0BP, UK

[#] Current address: Biosciences, College of Life and Environmental Sciences, University of Exeter, Stocker Road, Exeter, EX4 4QD, UK

*Corresponding author: p.j.hussey@durham.ac.uk

Summary

The cortical endoplasmic reticulum (ER) network in plants is a highly dynamic structure and it contacts the plasma membrane (PM) at ER/PM anchor/contact sites. These sites are known to be essential for communication between the ER and PM for lipid transport, calcium influx and ER morphology in mammalian and fungal cells. The nature of these contact sites is unknown in plants [1, 2] and here we have identified a complex that forms this bridge. This complex includes (i) NET3C which belongs to a plant specific super-family (NET) of actin-binding proteins [3]. (ii) VAP27, a plant homologue of the yeast Scs2 ER/PM contact site protein [4, 5] and (iii) the actin and microtubule networks. We demonstrate that NET3C and VAP27 localise to punctae at the PM, that NET3C and VAP27 form homodimers/oligomers and together form complexes with actin and microtubules. We show that F-actin modulates the turnover of NET3C at these punctae and microtubules regulate the exchange of VAP27 at the same sites. Based on these data, we propose a model for the structure of the plant ER/PM contact sites.

Highlights

1. NET3C belongs to a plant specific NET super-family.
2. NET3C links the actin cytoskeleton to ER/PM contact/anchor sites.
3. VAP27 is phylogenetically conserved and interacts with NET3C.
4. A novel complex for plant ER/PM contact site is identified from our study.

Results and Discussion

NET3C localises to ER/PM-associated punctae.

The actin cytoskeleton is a dynamic filament network that is involved in many cellular processes [6, 7]. In plants, it plays a unique role in organelle movement and endomembrane trafficking [8, 9], a role normally played by microtubules in animals [10, 11]. However, we know little about the proteins that are involved in linking the actin cytoskeleton to the plant endomembrane system. For example, it is known that the actin cytoskeleton is involved in ER movement but how they are linked is still an enigma. [12]. Substances made in the ER are transported to various destinations through vesicular trafficking pathways [13]. Although, direct association between ER and other membrane compartments also exists, which may provide alternative routes for material transport [14, 15]. In this context, the ER and PM are connected via ER/PM anchor/contact sites/junctions [16-19] but the nature of these sites in plants is unknown.

NET3C belongs to a plant specific NET super-family, which is a group of proteins that link the actin cytoskeleton to specific endomembrane compartments [3].The protein contains two functional domains (Figure 1A); a NAB (NET-Actin-Binding, a.a.1-94) domain and a coiled-coil domain (a.a.139-194). Here we show that NET3C binds F-actin. An actin co-sedimentation assay was performed using leaf extracts from *N. benthamiana* expressing GFP-NET3C. NET3C was found in the pellet fraction (lane4) in the presence of F-actin (Figure 1F). When expressed in *N. benthamiana* leaves, GFP-NET3C gave a 'beads on a string' localisation, which is a characteristic of members of the NET superfamily [3] (Figure 1B-D). The beads represent numerous immobile punctae (0.25-1.0μm) that appear to

associate with the ER (Figure 1B; Movie S1). These NET3C punctae resemble the ER punctae that were previously suggested to be putative ER/PM contact sites [1, 2, 20]

The association of NET3C punctae with the ER membrane was found to be independent of the actin cytoskeleton; 87.9±10.1% of NET3C punctae associated with the ER (Figure 1B) and when the cells were treated with the actin depolymerizing drug latrunculin B (Figure 1C), this association did not change significantly (87.4±8.3%; p=0.47). NET3C punctae are F-actin associated with 92.0±3.1% contacting the actin network (RFP-Lifact; Figure 1D). The NET3C punctae that are associated with the ER or F-actin compared to non-associated is significantly different (chi-square tests, $p<0.01$; Figure S1 A-C).

This association is further emphasized by showing that the turnover of NET3C punctae as assessed by FRAP, is influenced by F-actin but not by microtubules. The recovery of GFP-NET3C in the photo-beached region was enhanced significantly from 44.6±12.1% to 77.6±18.5% (max recovery, $p=1.03x10^{-7}$) when treated with latrunculin B (Figure 1E). In contrast, treatment of the cells with the microtubule depolymerizing drug, oryzalin, had little effect on NET3C turnover. These data indicate that NET3C localization is independent of F-actin but that once the punctae are attached to the F-actin, the exchange of NET3C is restrained.

As the ER association of NET3C is independent of actin and the interaction with actin is at the N-terminus of NET3C, we assessed whether the C-terminus is responsible for membrane localization. A NAB domain deleted NET3C was generated (NET3CΔNAB) and this is shown to localize to the ER and PM (Figure S1D-F), confirming that the C-terminus is essential for membrane localization. In addition, NET3C lacking the C-terminal sequence (NET3CΔC-term) did not associate with either F-actin or membrane compartments (Figure S1G).

In order to confirm that the localization of the GFP-NET3C in transiently expressing *N. benthamiana* cells is similar to the intracellular localization of native NET3C in Arabidopsis, immunofluorescence studies were performed

using anti-NET3C. Western-blotting using anti-NET3C identified a single band of the appropriate molecular weight in Arabidopsis cell extracts (Figure S1I).

Immunofluorescence was performed on Arabidopsis root tips expressing either GFP-HDEL(ER) or GFP-FABD2 (F-actin). Anti-NET3C labeled punctate structures that closely associate with the ER (96.4±5.6%, Figure 1H) and F-actin (96.2±7.3%, Figure S1H) at the cell cortex. Furthermore, immuno-gold labeling of Arabidopsis root tips showed gold particles at the PM in close proximity with the ER (Figure S1K) as well as at putative ER/PM contact sites (Figure 1G). The enrichment of anti-NET3C gold beads at the PM was confirmed statistically using chi-square tests (Figure S1L). These results on endogenous NET3C are consistent with the tobacco transient expression (Figure 1B), and confirm that NET3C is specifically found at punctae at the PM and putative ER/PM contact sites. Furthermore a double mutant, *NET3C RNAi/net3b* is shown to be gamete lethal indicating that NET3B/C are essential genes. (Figure S2C-F)

Studies in yeast have suggested that C-terminal basic motifs (lysine/arginine residues) in many proteins are required for phospholipid binding [21]. The sequence of the NET3C C-terminus encodes several lysine residues, including a lysine at position 211 (Figure 2A). A mutant where the lysine is substituted for alanine (GFP-NET3C K211A) was generated. This mutant is still able to form punctae that associate with F-actin and the ER (Figure 2B & F). However, most are mobile, which indicates that PM association is reduced (Movie S2). The ratio of fluorescence intensity at the cell cortex to the nucleoplasm was determined to be 10.9±4.1 (arbitrary units) for NET3C and 0.88±0.86 for NET3C-K211A (Figure 2E), indicating that the fluorescent signal for NET3C K211A accumulated in the nucleus, a feature of many cytoplasmic protein/FP constructs. [22, 23](Figure 2C-D).

When the GFP-NET3CΔNAB mutant, which on its own is evenly distributed on the ER and PM (Figure S1D), was expressed with full length RFP-NET3C, the deletion mutant was recruited to the punctae identified by the RFP-NET3C (Figure 2G). This indicates that native NET3C may exist as a dimer/oligomer through an interaction between the C-terminal sequences. This interaction was

confirmed by immunoprecipitation (Figure 2H) and FRET-FLIM experiments. In the FRET-FLIM, the lifetime of GFP-NET3C was found to be 2.21±0.03ns in the presence of RFP-NET3C, which is significantly reduced (by 0.24ns) when compared to GFP-NET3C on its own (2.45±0.03ns, $p=9.07x10^{-7}$), indicating a physical interaction [24, 25]. In comparison, the lifetime of the GFP-RFP fusion positive control was found to be 2.14±0.06ns (Figure 2I).

These data suggest a model where the NET3C dimerises/oligomerises at the C-terminal ends, the C-terminus binds the puncta to the membrane and the N-terminus binds F –actin. The association between NET3C and the PM is likely to be through direct lipid binding via the C-terminal basic motif or alternatively, through the interaction with other membrane localised proteins. NET3C is also likely to form anti-parallel dimers/oligomers that link the ER and PM as GFP-NET3CΔNAB localizes to the ER and PM. F-actin appears to stabilize the association of NET3C.(Figure 2J).

VAP27 localises to ER/PM contact sites

VAPs are phylogenetically conserved proteins [26-29]. They comprise a C-terminal transmembrane domain (a.a.234-253), an N-terminal major sperm domain (a.a.1-129) and a coiled-coil domain (a.a.178-234; Figure 3A). VAP27-YFP expressed in *N. benthamiana* leaves localises to the ER network as well as immobile punctate structures (0.25-1.2μm; Figure 3B), reminiscent of the putative ER/PM anchor sites observed in previous studies [1, 2] and in other organisms [17, 19]. These punctae are stationary while the majority of the ER network remodels (Figure S3A; Movie S3A). The VAP27-YFP punctae are located along ER tubules but not generally associated with three way junctions (Figure 3B). Stable Arabidopsis lines expressing VAP27-GFP under its endogenous promoter were generated, and the same ER associated punctae were identified (Figure S3B, Movie S3B). At the ultrastructural level, in Arabidopsis expressing VAP-27-YFP, attachment sites of the ER to PM were found. The sites are 0.5-1.0 μm, consistent with the size of VAP27 punctae observed using light microscopy (Figure S3C).

Yeast Scs2p is a known ER/PM contact site protein [4, 5, 16] and has 54% similarity to full length VAP27 (Figure S3E). When expressed in plants, Scs2p-GFP co-localized with VAP27-YFP at the ER and the putative ER/PM contact sites (Figure S3D). However, the Scs2p labeled ER/PM contact sites were less distinct, presumably because the two proteins compete at the same site. This result suggests that Scs2p co-localizes with VAP27 at equivalent ER/PM contact sites in plants.

Statistical analysis shows that 81.2±9.4% of VAP27-YFP labeled ER/PM contact sites associated with F-actin (GFP-Lifeact), whereas 59.5±4.3% were found to associate with KMD-RFP labeled microtubules[30] (Figure 3C-D). FRAP was used to study the dynamics of VAP27 turnover. ER membrane proteins (calnexin-GFP) exhibit a fast recovery at the ER cisternae ($T_{1/2}$=1.8-2.2 seconds) and has a large mobile fraction (Rmax=86-89%; Figure S3F). However, the recovery of VAP27-YFP at the ER/PM contact site was slow in comparison, with the maximum recovery reduced to 54.1±12.6% and a half-time of recovery of 15.0±7.6 seconds. The slow recovery suggests that VAP27 is part of a protein complex that affects its mobility. In addition, the turnover of VAP27-YFP dramatically increased when microtubules were depolymerized (Rmax=70.3±12.6%, p=0.006), indicating that VAP27 has some functional association with microtubules. On the other hand, recovery was unaffected when F-actin was removed (Rmax=49.9±10.4%; Figure 3E). These data indicate that the microtubule network has an impact on the dynamics of VAP27 at the ER/PM contact sites.

To further confirm an interaction between VAP27 and microtubules, total protein extracts from *N. benthamiana* leaves expressing VAP27-mRFP were co-incubated with microtubules and the mixture subjected to centrifugation. VAP27-mRFP was only detected in the pellet in the presence of microtubules (Figure 3F), confirming an interaction *in vitro*. This finding is consistent with the FRAP data described above. In conclusion, VAP27 is part of the ER/PM contact sites in plants and it associates with microtubules that constrain its mobility.

In addition, VAP27 is able to form dimers/oligomers *in vivo* like its mammalian equivalent[27], which was confirmed by immunoprecipitation (Figure S3G) and FRET-FLIM (Figure 3G). The lifetime of VAP27-GFP was reduced by 0.42ns to 2.06±0.1ns when co-expressed with VAP27-RFP which is significantly different from the VAP27-GFP control (2.48±0.04ns), indicating a physical interaction.

NET3C interacts with VAP27 at the ER/PM contact sites

The localisations of NET3C and VAP27 appear similar so we performed colocalisation studies. VAP27-YFP was co-expressed with CFP-HDEL (ER) and RFP-NET3C in *N. benthamiana* leaves and the results show that they co-localise at the ER/PM contact sites (Figure 4A). Interestingly, yeast Scs2-YFP also co-localised with NET3C at these contact sites, which further indicates that the localization of Scs2 in plant cells is the same as VAP27 (Figure S4A).

To investigate whether VAP27 and NET3C interact we used co-immunoprecipitation and FRET-FLIM. RFP-NET3C was found in the pellet fraction only when co-expressed with VAP27-YFP (Figure S4B) and the fluorescence lifetime of GFP-VAP27 was reduced by 0.29ns to 2.13±0.06 in the presence of RFP-NET3C compared to control (2.42ns±0.02). These data indicate a close association of NET3C/VAP27 *in vivo* (Figure 4B). Furthermore, immunostaining an Arabidopsis line stably transformed with 35S:VAP27-YFP using anti-NET3C and anti-GFP, showed that VAP27 punctae were also labeled with the NET3C antibody (Figure S4C).

The major sperm domain of VAP27 is conserved (Figure S3E) and previous studies suggest that a lysine residue at position 58 and two tyrosine residues at position 59/60 are necessary for VAP to interact with other proteins [29]. We mutated the lysine 58 and tyrosine 59/60 to asparagine and alanine respectively. The resulting mutants were still ER localised but failed to label any ER/PM contact sites (Figure 4C & S4D). Moreover, the mutants did not appear to co-localise with NET3C. This suggests that the mutation of these residues in the major sperm domain prevents the NET3C/VAP27 interaction and ER/PM association (Figure 4D).

Further mutagenesis was performed at the NET3C C-terminus (Figure 2A). Substitution of phenylalanine residues at positions 209 and 210 with alanine did not affect its interaction with VAP27 (Figure S4G). However, the association of NET3C F209/210A labelled punctae with F-actin was enhanced (Figure S4E-F), and the ER network was distorted (Figure S4H). In addition, the structure of VAP27 labelled ER/PM contact sites was also affected, as they became more mobile in the presence of NET3C F209/210A (Movie S5). These results suggest that specific residues at the C-terminus are essential for the association of NET3C with F-actin and membrane and they also appear to be important for maintaining ER structure.

NET3C-VAP27, Microtubule and Actin Model

Here we demonstrate that NET3C, VAP27 and the cytoskeleton are involved in organizing ER/PM contact/anchor sites (Figure 4E). We suggest two possible structural models explaining this association: (i) VAP27 may directly link the ER and PM and interact with PM/ER associated NET3C and as yet unknown PM proteins (Figure 4F). The actin and microtubule networks fix NET3C and VAP27 respectively at the contact sites; (ii) NET3C forms a pre-existing platform with other unknown proteins at the ER/PM and VAP27 is recruited to these sites upon certain signal stimuli or protein modification (Figure 4G). In both cases the cytoskeleton is responsible for stabilizing NET3C and VAP27 at the contact sites.

Figure legends

Figure 1. NET3C localises to PM/ER contact sites and F-actin.

(a) Diagrammatic illustration of the GFP-NET3C fusion; NET actin binding domain (a.a.1-a.a.94) and coiled-coil domain (a.a.139-a.a.194). **(B)** GFP-NET3C labelled immobile punctae co-locate along the ER (red) in leaf epidermal cells. NET3C punctae were associated (87.8 ± 10.1% of association) with the persistent ER nodules that are known as ER/PM contact sites (high magnification inset). **(C)** NET3C associates with the PM/ER contact sites independent of F-actin. When cells were treated with latrunculin (Lat B), NET3C punctae were associated with the ER network (87.4% ± 8.3 association). **(D)** NET3C punctae associate with F-actin (RFP-Lifact) producing a typical beads-on-string pattern (high magnification inset). Statistical analysis of NET3C punctae and F-actin association indicates a strong correlation (92.8 ± 3.1%). **(E)** Fluorescence-recovery after photobleaching (FRAP) of GFP-NET3C with different drug treatments. The mobility of GFP-NET3C was enhanced (reflected by an increase of max recovery) when actin filaments were removed with Lat B ($p=1.03x10^{-7}$). Little difference was found between oryzalin treatment (to remove microtubules) and the control (p=0.791). **(F)** Western blot probed with GFP-antibody showing co-sedimentation of GFP-NET3C with actin-filaments. After ultra-centrifugation, the supernatant (S) and pellet (P) fractions of GFP-NET3C with and without F-actin were fractionated on a gel. GFP-NET3C was found in the pellet fraction in the presence of F-actin. Lane 1, GFP-NET3C alone (S); Lane 2, GFP-NET3C alone (P); Lane 3, GFP-NET3C + F-actin (S); Lane 4, GFP-NET3C + F-actin (P). **(G)** Immuno-gold labeling of sections taken through Arabidopsis root tips using anti-NET3C showing NET3C associates with the PM as well as the ER/PM junctions. Gold particles were enhanced (larger dots overlaid on the original gold particles) using Photoshop for better visualisation. **(H)** Immuno-fluorescence of GFP-HDEL (ER marker) expressing Arabidopsis root tips with NET3C and GFP antibodies. Endogenous NET3C labels punctae and associates with the ER (96.4±5.6% association; scale bar = 10 μm for confocal; scale bar = 100 nm for TEM).

Figure 2. NET3C is able to self-interact and is recruited to the plasma membrane via the C-terminus.

(A) Diagrammatic illustration of NET3C showing the last ten amino, two phenoanalines (FF) are found at position 209/210 and a lysine (K) at 211. **(B**) Site-direct mutation of the C-terminal putative lipid binding motif on NET3C. GFP-NET3C K211A, which became

more cytoplasmically localised, labeled F-actin and mobile punctae. **(C) & (D)** Nuclear accumulation of GFP-NET3C K211A was found compared to control, indicating an enhanced cytoplasmic pool. The fluorescence intensity at the cell cortex and nuclear region are shown on the image. **(E)** Fluorescence ratio of cell cortex to nucleus . A high ratio (10.9±4.1) was found for GFP-NET3C, whereas a low ratio (0.88±0.86) was found with GFP-NET3C K211A. **(F)** Punctae labeled with GFP-NET3C K211A were still F-actin and ER associated. **(G)** GFP-NET3CΔNAB was recruited to the punctae when co-expressed with RFP-NET3C, suggesting that NET3C may self-interact through its C-terminal sequence. **(H)** Immuno-precipitation of RFP-NET3C and GFP-NET3C using a RFP antibody. GFP-NET3C was only found in the pellet fraction in the presence of RFP-NET3C (lane 1 and 2) indicating that the protein is able to self-interact. **(I)** FRET-FLIM analysis of NET3C interactions. Images were pseudo-coloured according to the GFP lifetime. The lifetime of GFP-NET3C (donor alone) was measured at 2.45±0.03 ns, whereas the lifetime of GFP was significantly reduced to 2.21±0.09 ns ($p=9.07x10^{-7}$) in the presence of RFP-NET3C (acceptor), suggesting NET3C is able to self-interact. In contrast, the positive control (GFP linked directly to RFP) had an average lifetime of 2.14±0.04 ns, indicating that a ca. 0.3ns reduction is found in a close association. The value of x^2 is close to 1 (indicative of good curve fitting) for all measurements. Please note that the peak of the lifetime frequency shifted to the left when the average fluorescence lifetime was reduced. **(J)** Diagram of possible plasma membrane recruitment of NET3C. NET3C dimer/oligomer binds to the PM or ER membrane via its C-terminus and binds to F-actin through the N-terminal NAB domain (I). NET3C could possibly form antiparallel dimers/oligomers that bridge between ER/PM (III). The K211A mutation prevents the membrane association of NET3C (II)&(IV) (scale bar = 10 μm).

Figure 3. VAP27 is an ER membrane protein and also localises to PM/ER contact sites

(A) Diagrammatic illustration of the VAP27-YFP fusion; major sperm domain (a.a.1-a.a.129), coiled-coil domain (a.a.178-a.a.234) and transmembrane domain (a.a.234-a.a.253). **(B)** VAP27-YFP localizes to the ER as well as PM/ER contact sites, Calnexin-GFP is a marker for the ER membrane (high magnification inset). **(C)** VAP27-YFP punctae at the ER/PM contact sites associate with F-actin (GFP-Lifact; 81.2±9.4% co-alignment; high magnification inset). **(D)** VAP27-YFP punctae associate with microtubules (KMD-RFP is the marker). Statistical analysis indicates a moderate ratio of co-alignment

(59.5±4.3%; high magnification inset). **(E)** Fluorescence-recovery after photobleaching (FRAP) of VAP27-YFP at the PM/ER contact sites following different drug treatments. The mobility of VAP27-YFP did not chang when actin filaments were removed with LAT B (p=0.465). A significant increase (reflected BY an increase in max recovery) was found with oryzalin treatment (p=0.006). **(F)** Western blot probed with RFP-antibody showing co-sedimentation of VAP27-mRFP with microtubules. After ultra-centrifugation, the supernatant (S) and pellet (P) fractions in the presence or absence of microtubules were run on the gel. VAP27 was found in the pellet fraction in the presence of microtubules. Lane 1, VAP27-RFP + MT (S); Lane 2, VAP27-RFP + MT (P); Lane 3, VAP27-RFP alone (S); Lane 4, VAP27-RFP alone (P). **(G)** FRET-FLIM analysis of VAP27 interaction. The lifetime of VAP27-GFP (donor alone) was measured at 2.48±0.04ns, whereas the lifetime of GFP was significantly reduced to 2.06±0.01ns ($p=3.49 \times 10^{-9}$) in the presence of VAP27-RFP (scale bar = 10 μm).

Figure 4. VAP27 interacts with NET3C.

(A)The ER network was labeled by CFP-HDEL and RFP-NET3C co-localised with VAP27-YFP at the ER/PM contact sites. **(B)** FRET-FLIM analysis of the NET3C/VAP27 interaction. GFP-VAP27 has a lifetime of 2.42±0.02ns on its own. The fluorescence lifetime of GFP-VAP27 was reduced to 2.13±0.06 ns ($p=1.23 \times 10^{-12}$) when co-expressed with RFP-NET3C, indicating an interaction between the two proteins. **(C)** Site-directed mutation in the major sperm domain. VAP27 T59/60A was still found at the ER network but failed to concentrate at the ER/PM contact site and to colocalise with RFP-NET3C. **(D)** Propose illustration of VAP27-PM association. Point mutations on the major sperm domain prevent VAP27 associating with PM/ER contact site. **(E)** Diagram showing VAP27 (at the ER) interacting with NET3C (at the PM), forming a stationary complex at the ER/PM contact site. The cytoskeleton was found associated with these complexes interacting with NET3C and VAP27. Two possible models are suggested: **(F)** VAP27 may directly link the ER/PM and interact with PM associated NET3C.;**(G)** Alternatively, NET3C may form a pre-existing platform with other proteins at the plasma membrane. In addition to NET3C and VAP27, other proteins may also be required for the function and structure of ER/PM contact sites (scale bar = 10 μm).

Accession number

The Arabidopsis genome accession number for NET3C is At2g47920 and for VAP27 it is At3g60600.

Acknowledgements

We thank Dr Andrei Smertenko for helping with the microtubule co-sedimentation assay. We also thank Patrick Duckney for providing the GFP-RFP construct. The work was supported by a BBSRC grant (BB/G006334/1) to P.J.H. and preliminary work on VAP27 was supported by a Leverhulme trust grant (F/00382/G) to C.H.

Author Contributions

P.W. performed the experiments.. T.J.H., I.C. , M.J.D, C.R., and IS contributed data and helped in the analysis. P.W., C.H. and P.J.H. wrote the manuscript.

References

1. Sparkes, I., Runions, J., Hawes, C., and Griffing, L. (2009). Movement and remodeling of the endoplasmic reticulum in nondividing cells of tobacco leaves. Plant Cell *21*, 3937-3949.
2. Sparkes, I., Hawes, C., and Frigerio, L. (2011). FrontiERs: movers and shapers of the higher plant cortical endoplasmic reticulum. Curr Opin Plant Biol *14*, 658-665.
3. Deeks, M.J., Calcutt, J.R., Ingle, E.K., Hawkins, T.J., Chapman, S., Richardson, A.C., Mentlak, D.A., Dixon, M.R., Cartwright, F., Smertenko, A.P., et al. (2012). A superfamily of actin-binding proteins at the actin-membrane nexus of higher plants. Curr Biol *22*, 1595-1600.
4. Stefan, C.J., Manford, A.G., Baird, D., Yamada-Hanff, J., Mao, Y., and Emr, S.D. (2011). Osh proteins regulate phosphoinositide metabolism at ER-plasma membrane contact sites. Cell *144*, 389-401.
5. Loewen, C.J., Young, B.P., Tavassoli, S., and Levine, T.P. (2007). Inheritance of cortical ER in yeast is required for normal septin organization. J Cell Biol *179*, 467-483.
6. Hussey, P.J., Ketelaar, T., and Deeks, M.J. (2006). Control of the actin cytoskeleton in plant cell growth. Annu Rev Plant Biol *57*, 109-125.
7. Smertenko, A.P., Deeks, M.J., and Hussey, P.J. (2010). Strategies of actin reorganisation in plant cells. J Cell Sci *123*, 3019-3028.
8. Boevink, P., Oparka, K., Santa Cruz, S., Martin, B., Betteridge, A., and Hawes, C. (1998). Stacks on tracks: the plant Golgi apparatus traffics on an actin/ER network. Plant J *15*, 441-447.
9. Ueda, H., Yokota, E., Kutsuna, N., Shimada, T., Tamura, K., Shimmen, T., Hasezawa, S., Dolja, V.V., and Hara-Nishimura, I. (2010). Myosin-dependent endoplasmic reticulum motility and F-actin organization in plant cells. Proc Natl Acad Sci U S A *107*, 6894-6899.
10. Klopfenstein, D.R., Kappeler, F., and Hauri, H.P. (1998). A novel direct interaction of endoplasmic reticulum with microtubules. The EMBO journal *17*, 6168-6177.
11. Watson, P., Forster, R., Palmer, K.J., Pepperkok, R., and Stephens, D.J. (2005). Coupling of ER exit to microtubules through direct interaction of COPII with dynactin. Nat Cell Biol *7*, 48-55.
12. Sparkes, I.A., Frigerio, L., Tolley, N., and Hawes, C. (2009). The plant endoplasmic reticulum: a cell-wide web. Biochem J *423*, 145-155.
13. Bonifacino, J.S., and Glick, B.S. (2004). The mechanisms of vesicle budding and fusion. Cell *116*, 153-166.
14. Schattat, M., Barton, K., Baudisch, B., Klosgen, R.B., and Mathur, J. (2011). Plastid stromule branching coincides with contiguous endoplasmic reticulum dynamics. Plant physiology *155*, 1667-1677.
15. de Brito, O.M., and Scorrano, L. (2008). Mitofusin 2 tethers endoplasmic reticulum to mitochondria. Nature *456*, 605-610.
16. Manford, A.G., Stefan, C.J., Yuan, H.L., Macgurn, J.A., and Emr, S.D. (2012). ER-to-plasma membrane tethering proteins regulate cell signaling and ER morphology. Dev Cell *23*, 1129-1140.
17. Varnai, P., Toth, B., Toth, D.J., Hunyady, L., and Balla, T. (2007). Visualization and manipulation of plasma membrane-endoplasmic reticulum contact sites indicates the presence of additional molecular components within the STIM1-Orai1 Complex. J Biol Chem *282*, 29678-29690.

18. Luik, R.M., Wang, B., Prakriya, M., Wu, M.M., and Lewis, R.S. (2008). Oligomerization of STIM1 couples ER calcium depletion to CRAC channel activation. Nature *454*, 538-542.
19. Giordano, F., Saheki, Y., Idevall-Hagren, O., Colombo, S.F., Pirruccello, M., Milosevic, I., Gracheva, E.O., Bagriantsev, S.N., Borgese, N., and De Camilli, P. (2013). PI(4,5)P(2)-dependent and Ca(2+)-regulated ER-PM interactions mediated by the extended synaptotagmins. Cell *153*, 1494-1509.
20. Sparkes, I.A., Ketelaar, T., de Ruijter, N.C., and Hawes, C. (2009). Grab a Golgi: laser trapping of Golgi bodies reveals in vivo interactions with the endoplasmic reticulum. Traffic *10*, 567-571.
21. Scheglmann, D., Werner, K., Eiselt, G., and Klinger, R. (2002). Role of paired basic residues of protein C-termini in phospholipid binding. Protein Eng *15*, 521-528.
22. Brandizzi, F., Hanton, S., DaSilva, L.L., Boevink, P., Evans, D., Oparka, K., Denecke, J., and Hawes, C. (2003). ER quality control can lead to retrograde transport from the ER lumen to the cytosol and the nucleoplasm in plants. Plant J *34*, 269-281.
23. Wang, R., and Brattain, M.G. (2007). The maximal size of protein to diffuse through the nuclear pore is larger than 60kDa. FEBS Lett *581*, 3164-3170.
24. Schoberer, J., Liebminger, E., Botchway, S.W., Strasser, R., and Hawes, C. (2013). Time-resolved fluorescence imaging reveals differential interactions of N-glycan processing enzymes across the Golgi stack in planta. Plant physiology *161*, 1737-1754.
25. Osterrieder, A., Carvalho, C.M., Latijnhouwers, M., Johansen, J.N., Stubbs, C., Botchway, S., and Hawes, C. (2009). Fluorescence lifetime imaging of interactions between golgi tethering factors and small GTPases in plants. Traffic *10*, 1034-1046.
26. Lev, S., Ben Halevy, D., Peretti, D., and Dahan, N. (2008). The VAP protein family: from cellular functions to motor neuron disease. Trends Cell Biol *18*, 282-290.
27. Nishimura, Y., Hayashi, M., Inada, H., and Tanaka, T. (1999). Molecular cloning and characterization of mammalian homologues of vesicle-associated membrane protein-associated (VAMP-associated) proteins. Biochem Biophys Res Commun *254*, 21-26.
28. Saravanan, R.S., Slabaugh, E., Singh, V.R., Lapidus, L.J., Haas, T., and Brandizzi, F. (2009). The targeting of the oxysterol-binding protein ORP3a to the endoplasmic reticulum relies on the plant VAP33 homolog PVA12. Plant J *58*, 817-830.
29. Loewen, C.J., and Levine, T.P. (2005). A highly conserved binding site in vesicle-associated membrane protein-associated protein (VAP) for the FFAT motif of lipid-binding proteins. J Biol Chem *280*, 14097-14104.
30. Deeks, M.J., Fendrych, M., Smertenko, A., Bell, K.S., Oparka, K., Cvrckova, F., Zarsky, V., and Hussey, P.J. (2010). The plant formin AtFH4 interacts with both actin and microtubules, and contains a newly identified microtubule-binding domain. J Cell Sci *123*, 1209-1215.

Figure 1

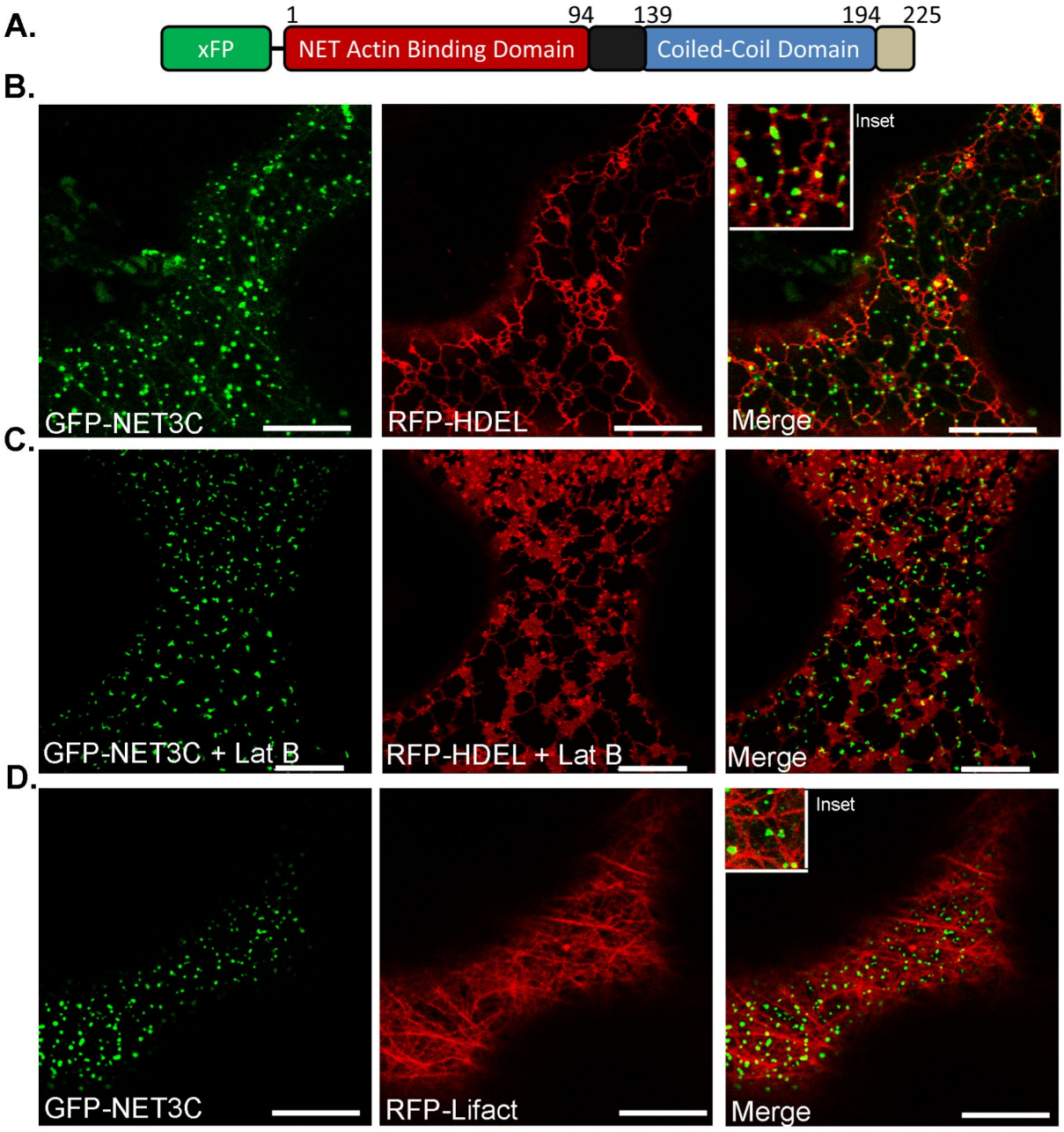

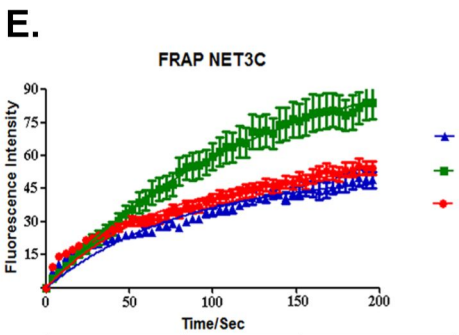

	Max Recovery (%)	Halftime of Recovery (s)
GFP-NET3C	44.55 ± 12.06	80.87 ± 37.9
GFP-NET3C + LatB	77.58 ± 18.5	91.27 ± 20.8
GFP-NET3C + Ory	43.62 ± 4.54	60.91 ± 24.49

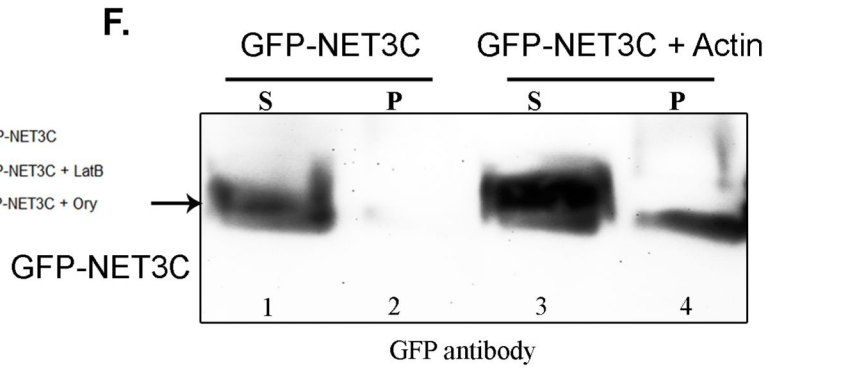

1. GFP-NET3C only, supernatant
2. GFP-NET3C only, pellet
3. GFP-NET3C + Actin, supernatant
4. GFP-NET3C + Actin, pellet

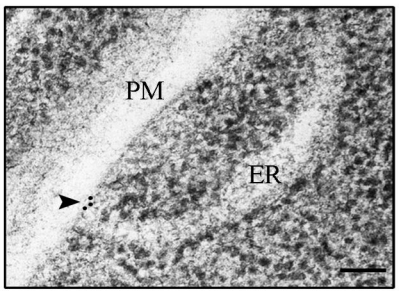

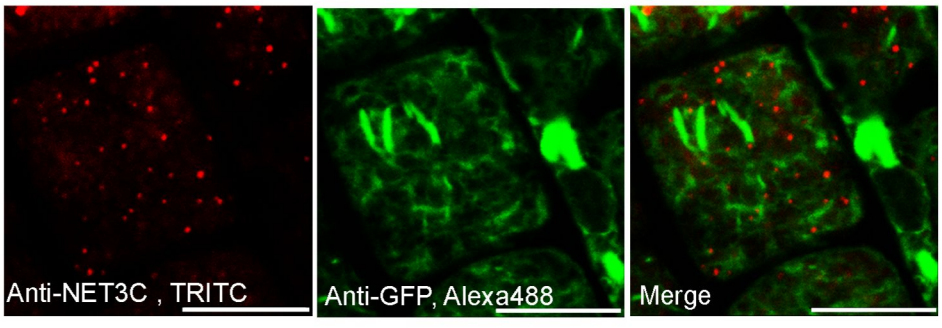

A.

B.

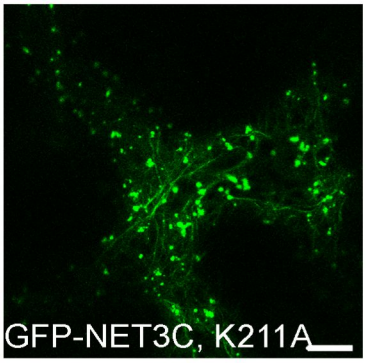

C.

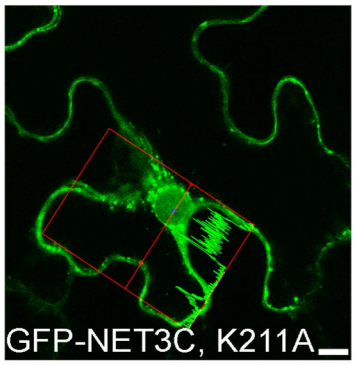

D.

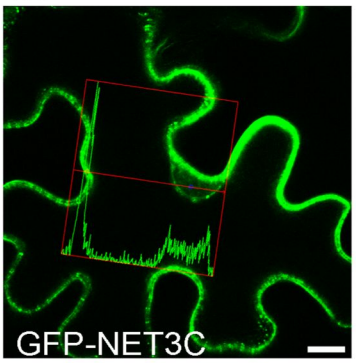

E.

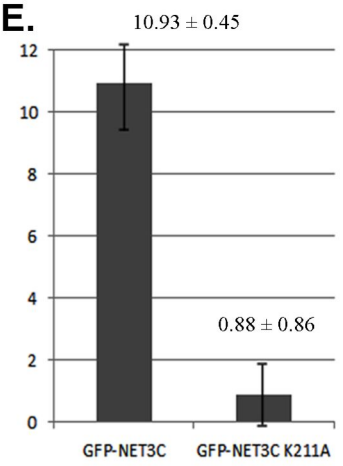

Flourescent intensity ratio
Peripheral/Nuclear

F.

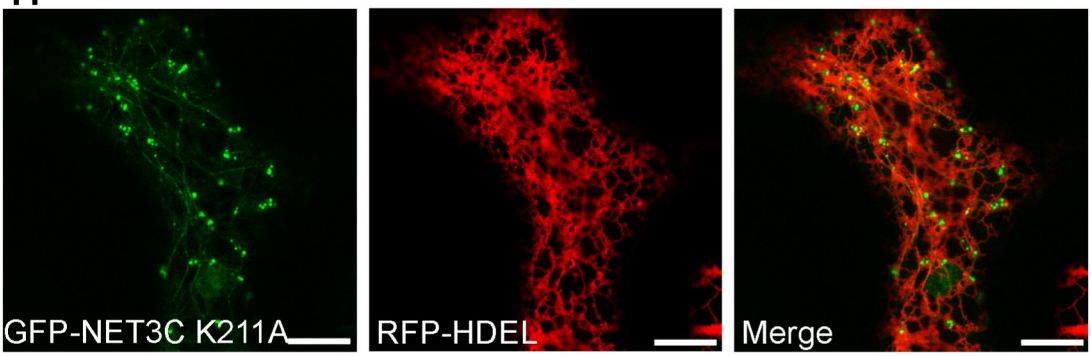

G.

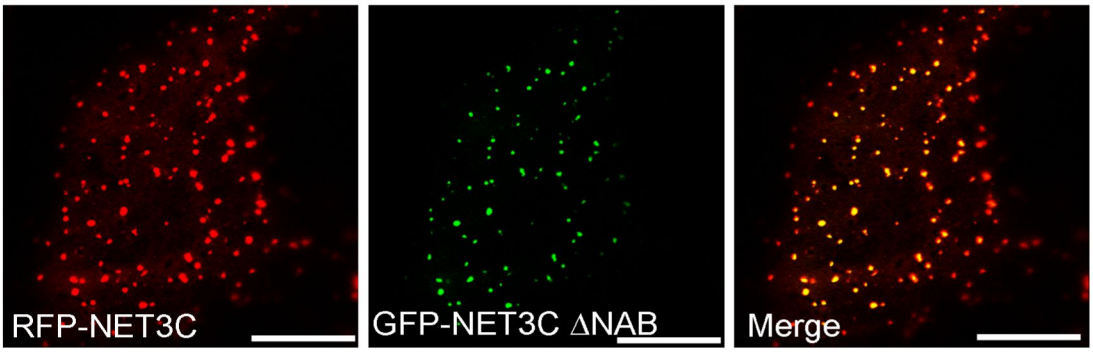

H.

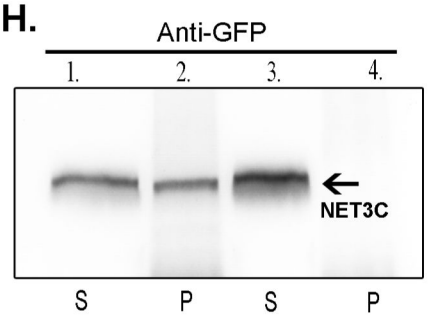

1. RFP-NET3C + GFP-NET3C, Supernatant
2. RFP-NET3C + GFP-NET3C, Pellet
3. GFP-NET3C, Supernatant
4. GFP-NET3C Pellet

I.

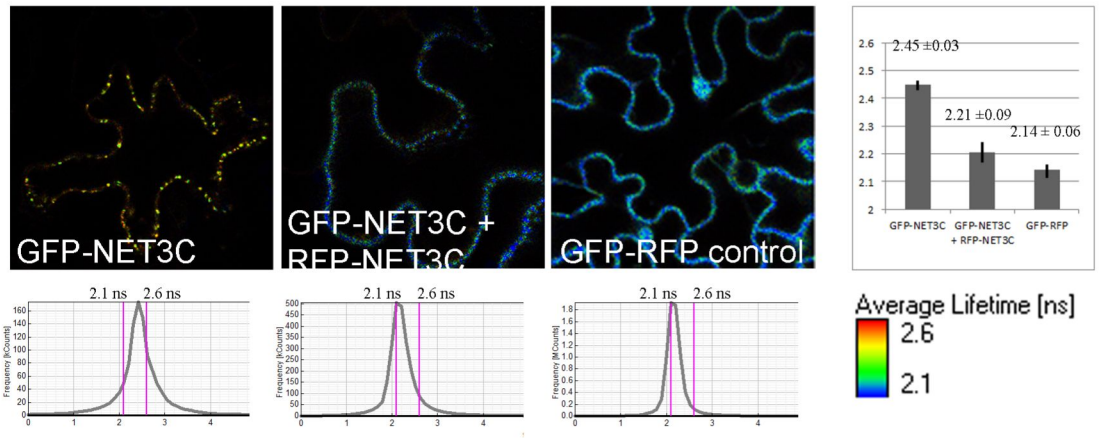

J.

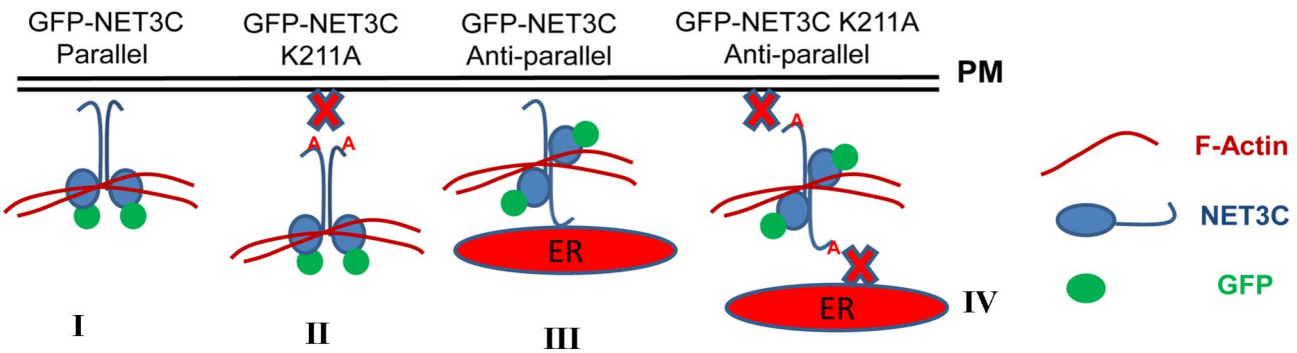

Figure 3

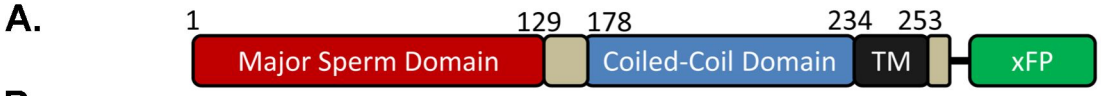

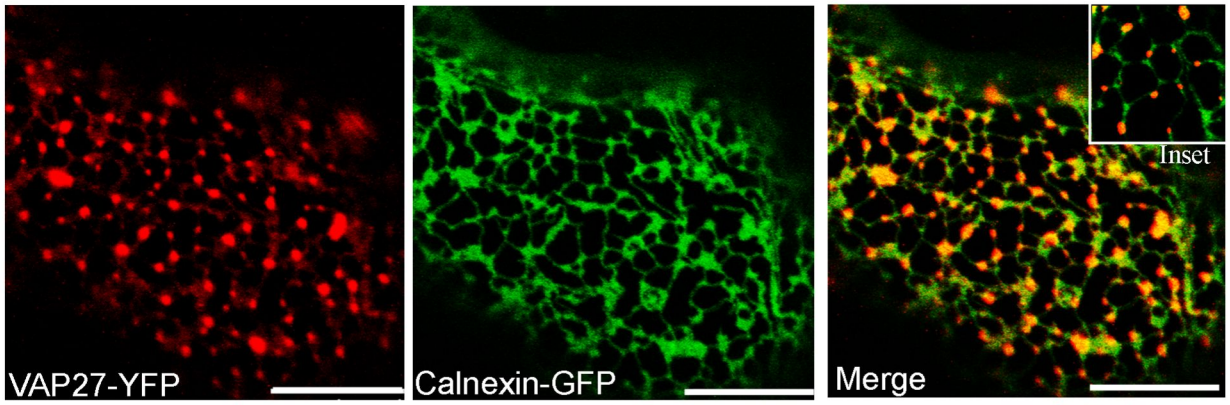

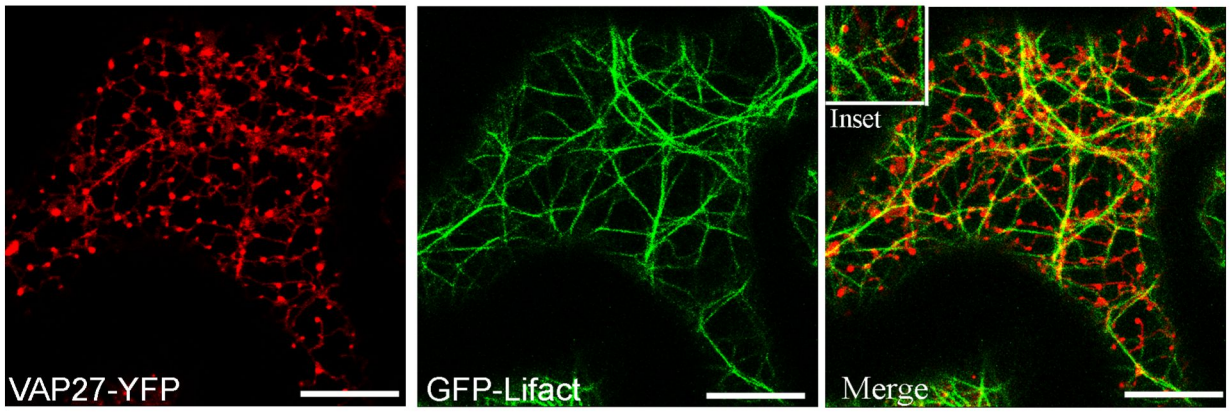

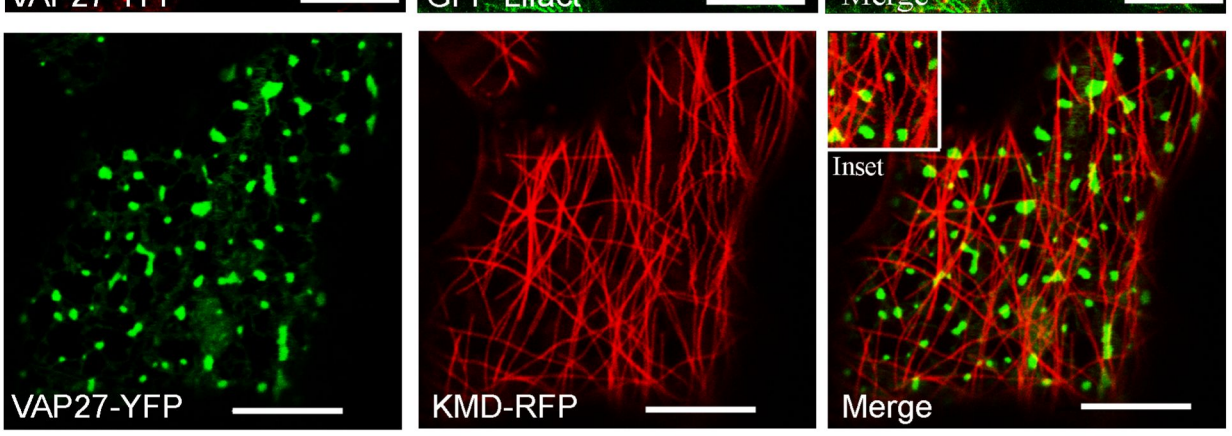

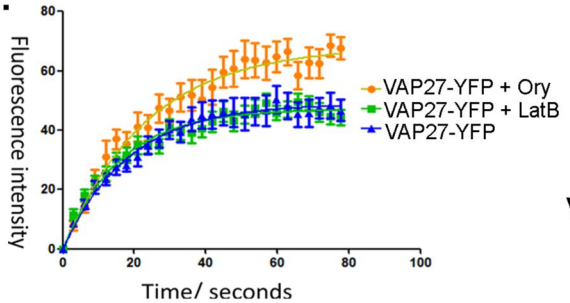

	Max Recovery (%)	Half Time (s)
VAP27-YFP	54.09 ± 12.55	14.95 ± 7.62
VAP27-YFP + LatB	49.87 ± 10.38	11.86 ± 4.03
VAP27-YFP + Ory	70.27 ± 16.33	18.16 ± 9.52

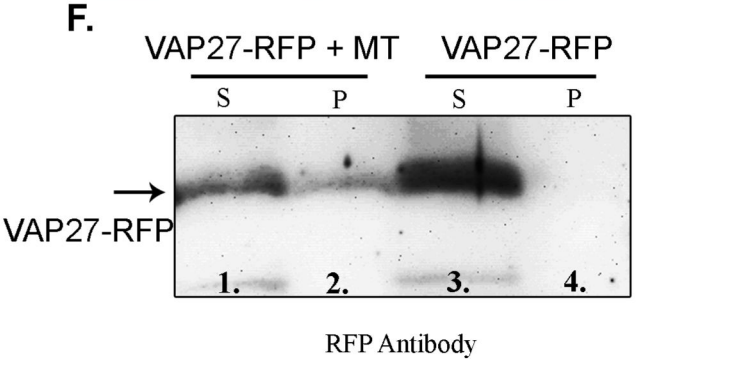

1. VAP27 + MT, supernatant
2. VAP27 + MT, pellet
3. VAP27 only, supernatant
4..VAP27 only, pellet

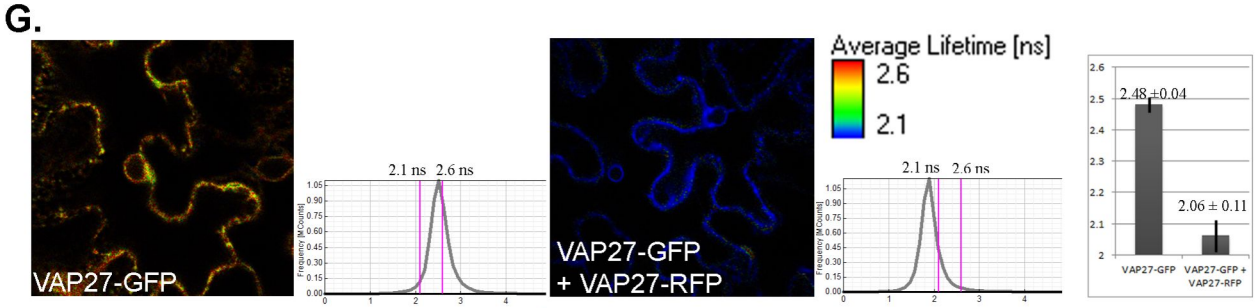

Figure 4

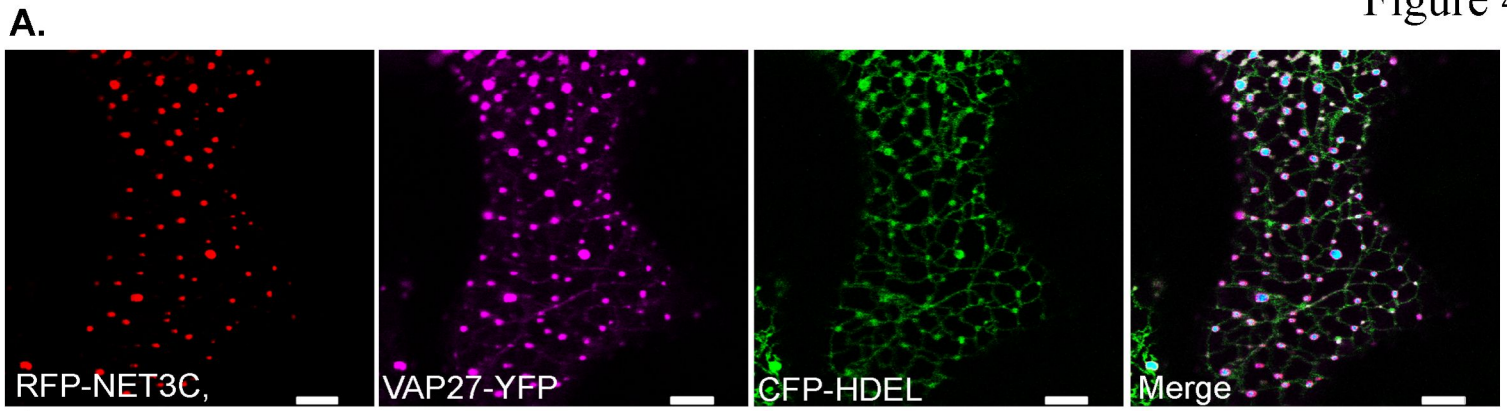
A.
RFP-NET3C,
VAP27-YFP
CFP-HDEL
Merge

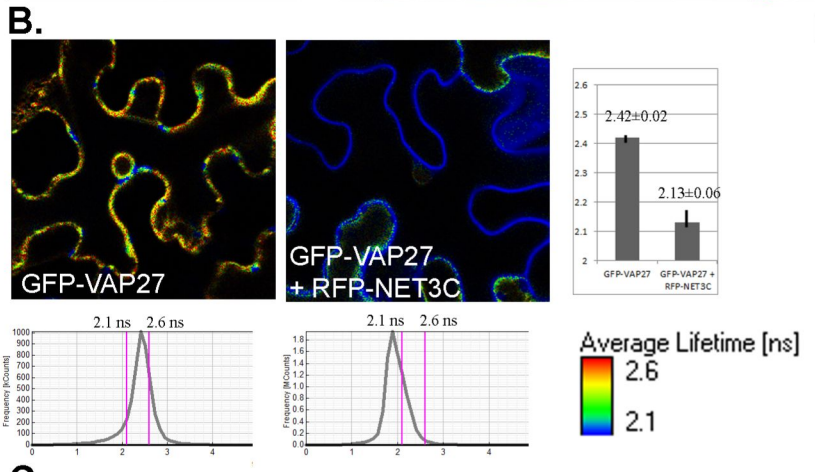
B.
GFP-VAP27
GFP-VAP27
+ RFP-NET3C
2.42±0.02
2.13±0.06
GFP-VAP27
GFP-VAP27 + RFP-NET3C
2.1 ns
2.6 ns
2.1 ns
2.6 ns
Average Lifetime [ns]
2.6
2.1

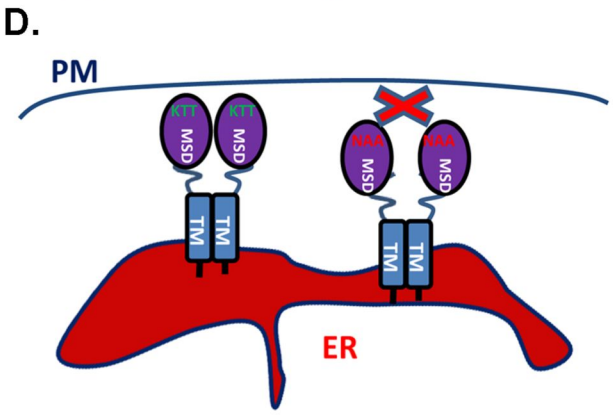
D.
PM
KTT
MSD
TM
NAA
ER

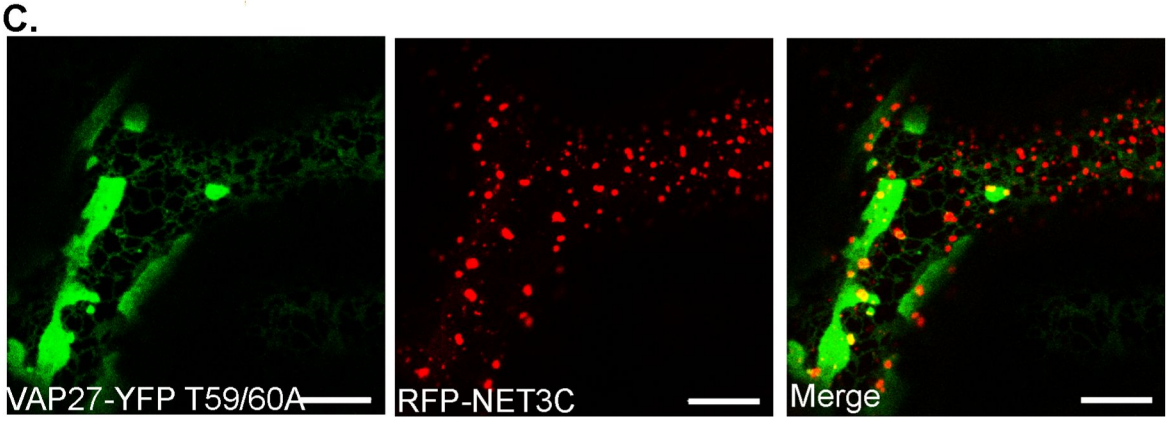
C.
VAP27-YFP T59/60A
RFP-NET3C
Merge

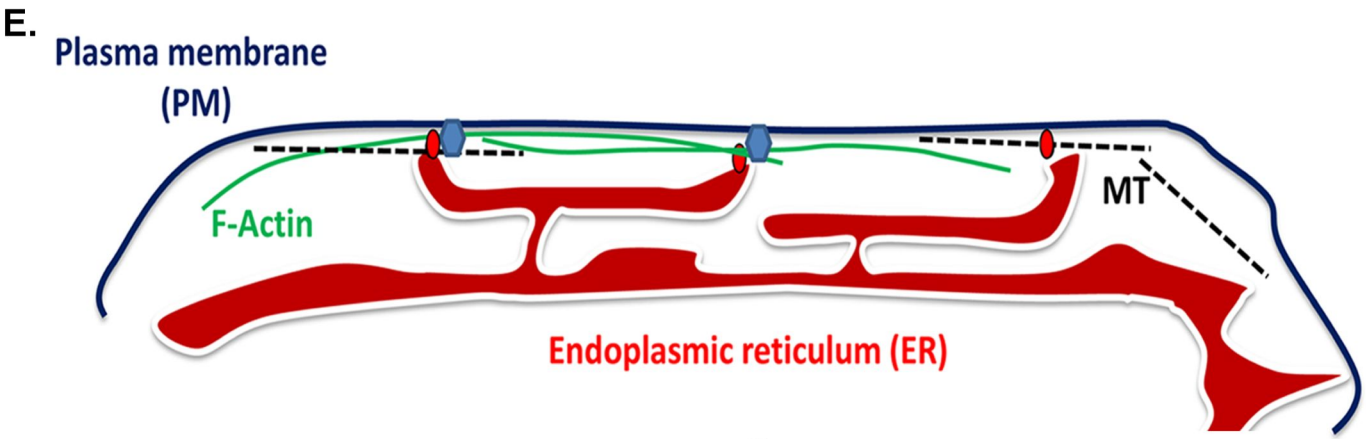
E.
Plasma membrane
(PM)
F-Actin
MT
Endoplasmic reticulum (ER)

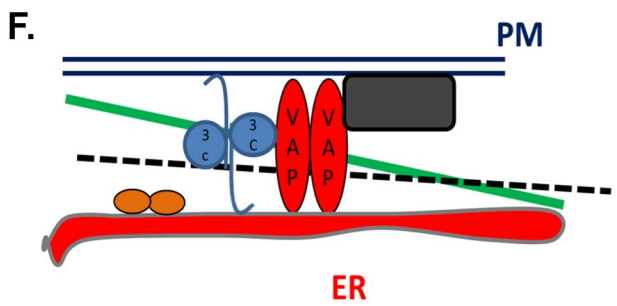
F.
PM
3 c
3 C
V A P
ER

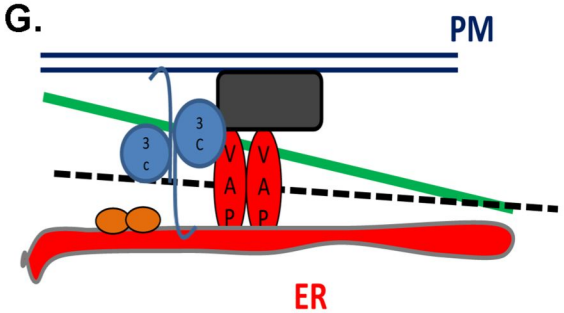
G.
PM
3 c
3 C
V A P
ER


Unknown ER proteins
Unknown PM proteins
F-Actin
Microtubules

Figure S1

A.

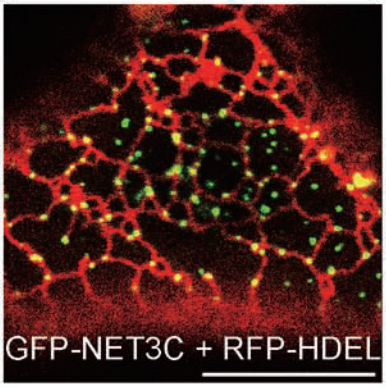

B.

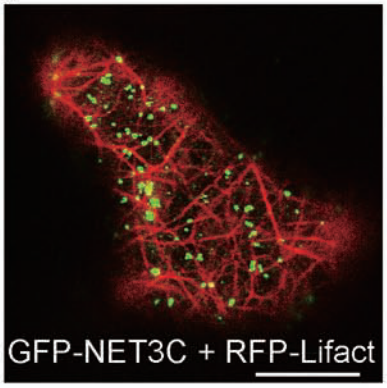

C.

Association of NET3C with ER (A)				
	n	Density (per 100µm²)	Expect if random distribution	p Value
Non-ER associated	23	14.4	92.5	4.831 2E-26
ER associated	151	107.9	81.5	
Association of NET3C with F-actin (B)				
Non-Actin associated	11	6.1	41.7	1E-6
Actin associated	86	35.8	55.3	

D.

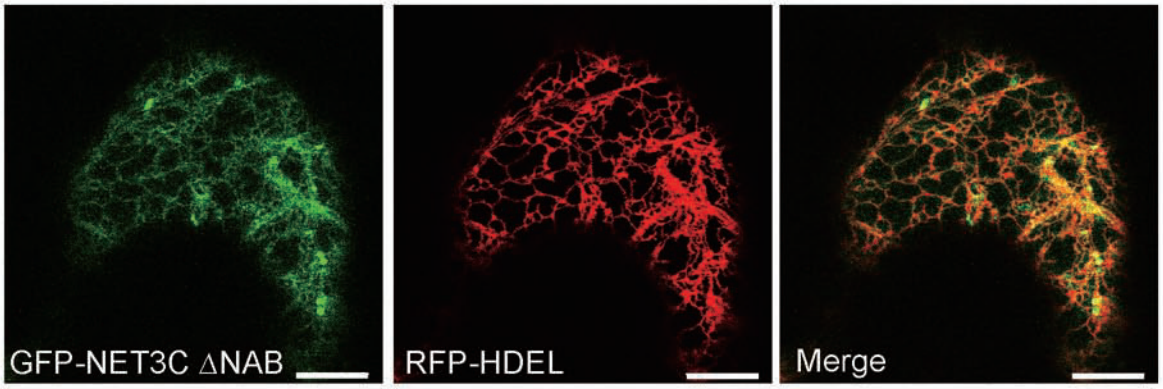

E.

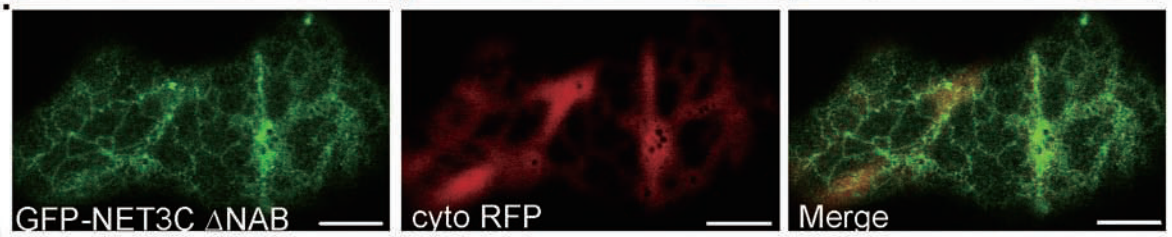

G.

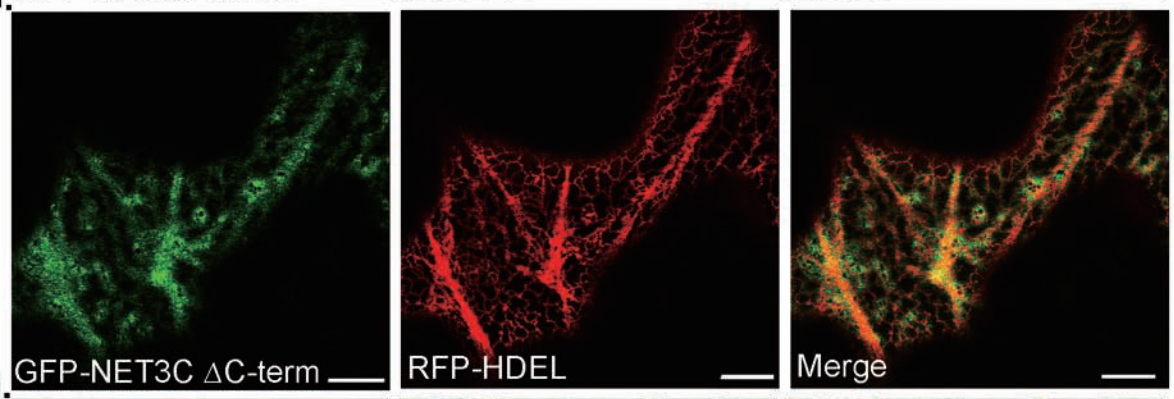

H.

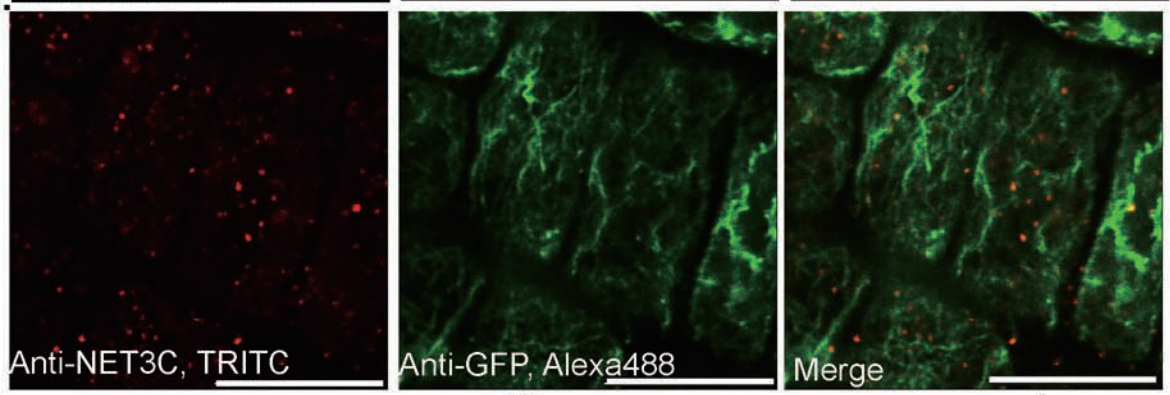

F.

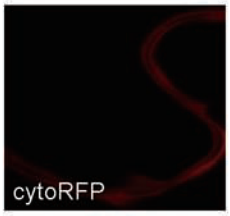

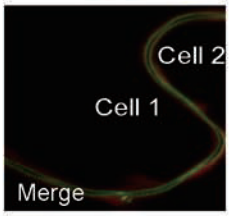

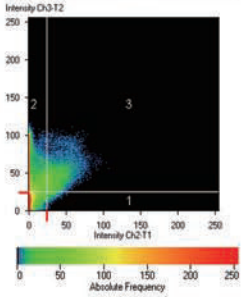

Pearson's correlation
Rp = 0.37

I.

J.

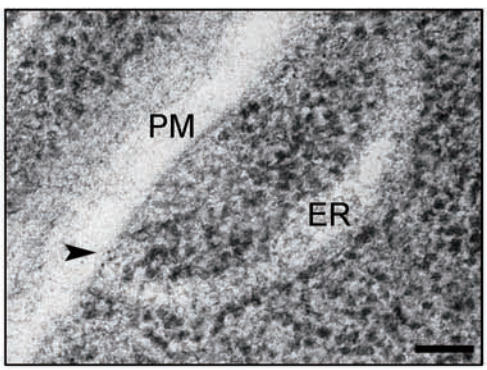

K.

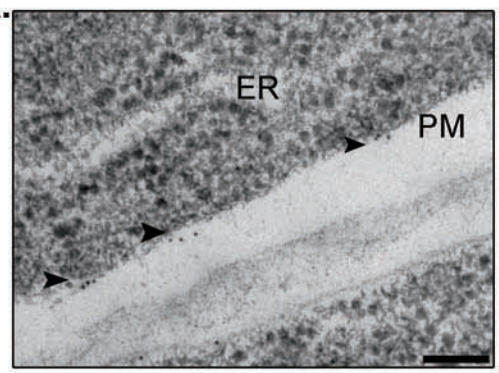

L.

Association of NET3C gold beads with PM				
	n	Density (per µm²)	Expect if random distribution	p Value
PM localised	103	54.8	16.2	0
Cytoplasm localised	40	2.7	126.8	

Figure S1. NET3C punctae distribution is enriched at the ER and PM, and its C-terminal sequence is essential for this localisation. Related to Figure 1 & 2.

(A)-(C) Analysis of NET3C co-alignment with the ER network (A) or F-actin (B) using chi-square tests. The distribution of NET3C punctae were scored as ER-associated or non-ER associated over 303.5μm^2. The association of NET3C on the ER network (151/23) is significantly different from that were the distribution to be random (91.5/82.5; p=4.83x10^{-26}). Similarly, the distribution of NET3C punctae with F-actin was performed in the same way showing that their association is not random (p= 1x10^{-06}). **(D)** NET3C lacking the NAB domain (NET3CΔNAB) was not able to bind to actin. GFP-NET3CΔNAB localized evenly to the ER network as well as the plasma membrane. **(E)** GFP-NET3CΔNAB co-expressed with cytosolic RFP. The PM fluorescence labeled by GFP-NET3CΔNAB (green) is distinct from cytosolic RFP (red). **(F)** The Pearson's correlation of co-localisation at cell cortex was measured at 0.37 (indicating a medium level of correlation), suggesting that GFP-NET3CΔNAB and cytosolic RFP are partially co-localised. **(G)** NET3C lacking the C-terminal sequence (GFP-NET3CΔC-term) is cytosolic, suggesting that this sequence is essential for both membrane and F-actin association. **(H)** Immuno-fluorescence of GFP-FABD2 (F-actin marker) expressing Arabidopsis root tips with NET3C and GFP antibodies. Endogenous NET3C forms punctae and associates with the actin cytoskeleton (96.2% association). **(I)** Western blot of total Arabidopsis seedling protein using a polyclonal NET3C antibody (1:500 dilution) showing a clear band at 25 kDa. **(J)** Original of Figure 1F without enhancement. Gold particles were found at the plasma membrane as well as the ER/PM junctions. **(K)** Immuno-gold labeling of NET3C in Arabidopsis root tips, gold particles were found at the PM as well as in a close proximity with the ER. **(L)** A total number of 143 anti-NET3C gold particles (from 14 individual EM images) were analyzed; the distribution of gold between the cytoplasm and the plasma membrane was compared. The p value calculated from chi-square tests indicate that gold particles are enriched at the plasma membrane. (scale bar = 10 μm for confocal; scale bar = 100 nm for TEM).

Figure S2

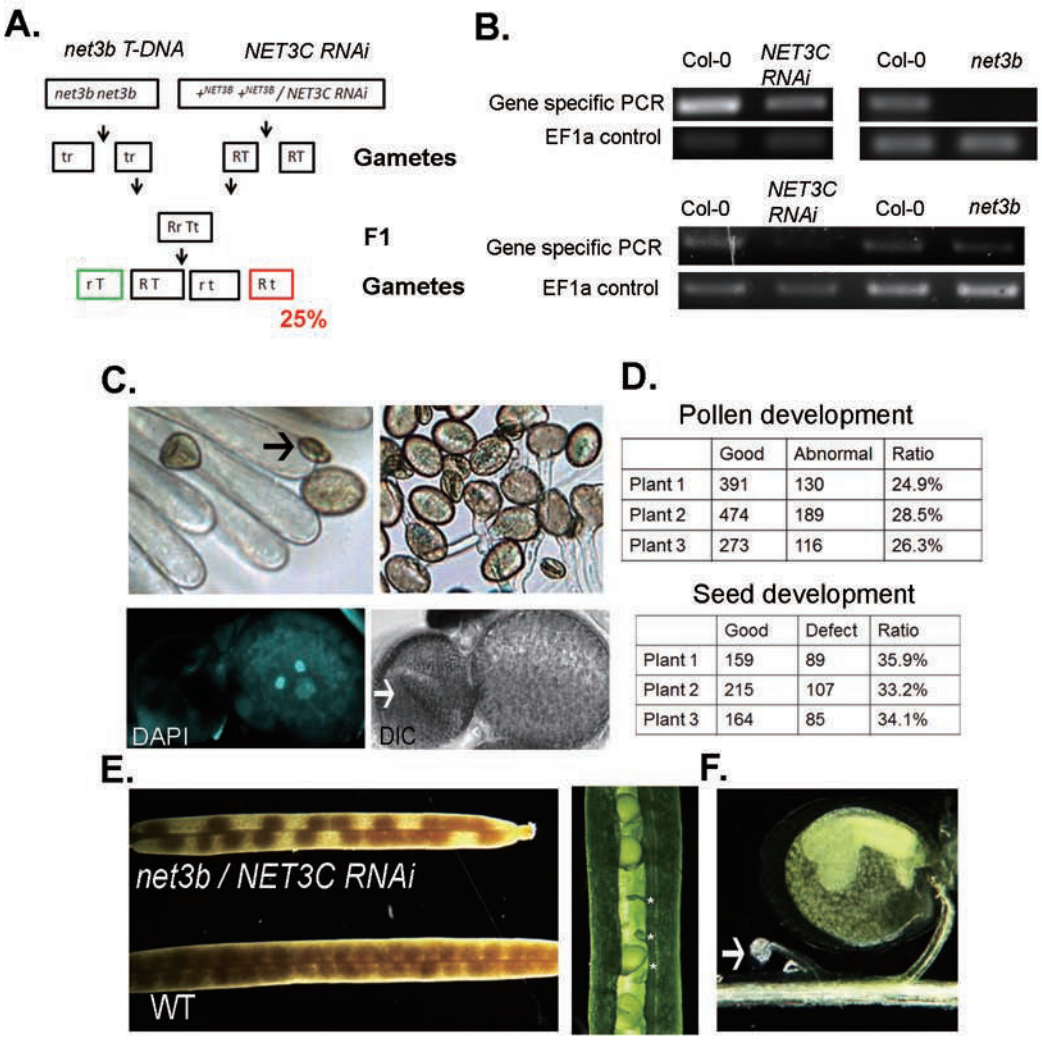

	Good	Abnormal	Ratio
Plant 1	391	130	24.9%
Plant 2	474	189	28.5%
Plant 3	273	116	26.3%

	Good	Defect	Ratio
Plant 1	159	89	35.9%
Plant 2	215	107	33.2%
Plant 3	164	85	34.1%

Figure S2. NET3C localises to PM/ER contact sites and with NET3B is essential for normal development. Related to Figure 1 & 2.

(A) Graphic illustration of the genetic segregation of the *NET3C RNAi/net3b* double mutant (*NET3C RNAi* (AGRIKOLA)*/net3b* (SALK_129238C)). Pollen (RT) from the *NET3C RNAi* line was used to pollinate the *net3b T-DNA* homozygous line (rt), producing the F1 generation that contains both alleles (RrTt). A quarter of the haploid are homozygous for both *NET3C RNAi* and *net3b T-DNA* (Rt). **(B)**First-strand cDNA from various NET3 mutants was used for RT-PCR. In the single mutants, the transcription of NET3C was significantly knocked-down, whereas full length NET3B transcripts were completely disrupted (upper panel). In the *NET3C RNAi/net3b-1* double mutant (lower panel), the NET3C transcript was knocked-down and had no effect on NET3B, indicating *NET3C RNAi* allele is dominant and *net3b-1 T-DNA* is recessive. **(C)** Some pollen grains from *NET3C RNAi/net3b-1* double mutant were abnormal (arrow) and unable to germinate. The defective pollen do not contain any DNA as indicated by DAPI staining. The development of pollen showed an average ca. 25% abnormality, which is in agreement with the prediction that a quarter of haploid cells inherit both alleles. **(D)** Statistical analysis of pollen and seed development in *NET3C RNAi/net3b* double mutant. Three individual plants were analyzed and the ratio of abnormality is shown in the table. **(E)** Siliques from *NET3C RNAi/net3b-1* double mutant contain a number of non-developed seeds. **(F)** The development of those seeds is disrupted at a very early stage. About 34% of seed development is disrupted at the early ovule stage. A similar phenotype (34.6% non-developed seeds, n>500) was observed when the *NET3C RNAi/net3b* double heterozygote was crossed with wild-type pollen, indicating the defect in seed development is likely to be at the haploid stage.

Figure S3

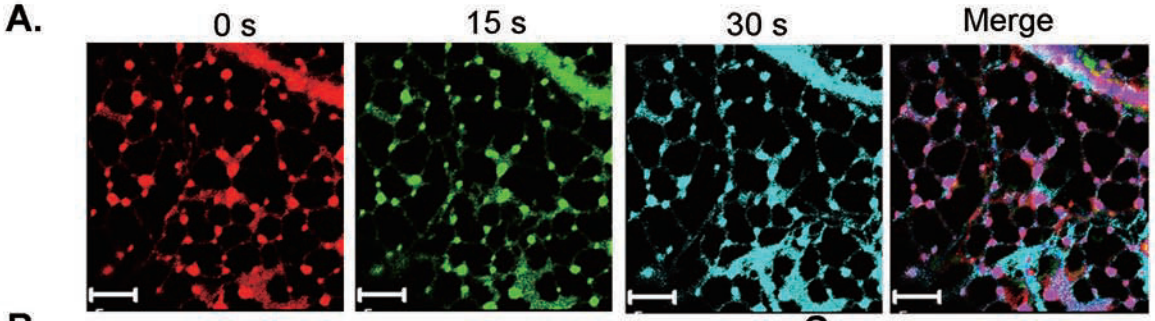

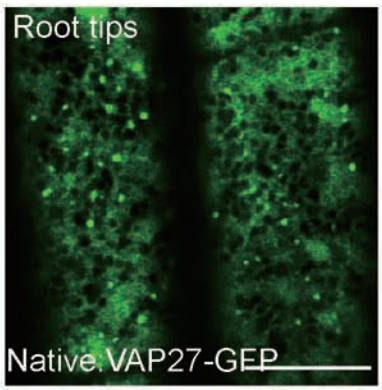

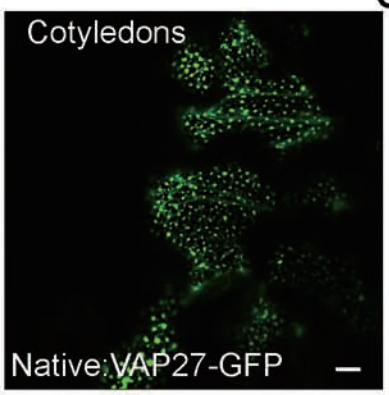

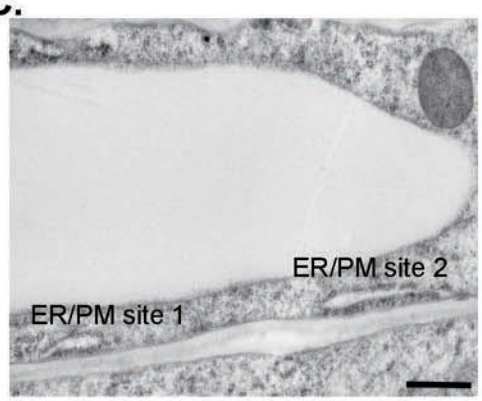

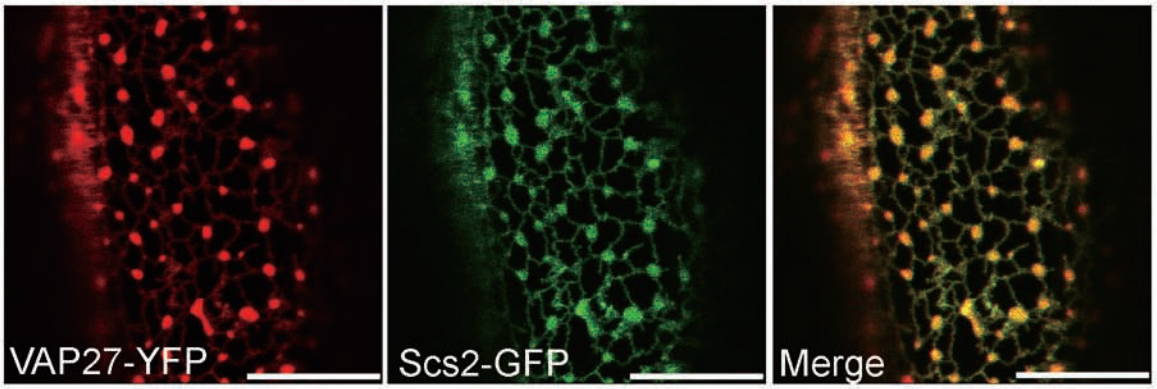

E.

```
Scs2    ---MSAVEISPDVLVYKSPLTEQSTEYASISNNSDQTIAFKVKTTAPKFYCVRPNAAVVA
VAP27   MSNSELLTVEPLDLQFPFELKKQISCSLYLTNKTDNNVAFKVKTTNPKKYCVRPNTGVVL
            . : :.*  * :   *.:* :    ::*::*:.:******* ** ******:.**

Scs2    PGETIQVQVIFLGLTEEPAADFKCRDKFLVITLPSPYDLNGKAVADVWSDLEAEFKQQAI
VAP27   PRSTCEVLVTMQAQKEAP-SDMQCKDKFLLQGVIASPGVTAKEVTPEMFSKEAGHRVEET
        * .* :* * : . .* * :*::*:****:  : :. .:..* *:    . ** .: :

Scs2    SKKIKVKYLISPDVHPAQNQNIQENKETVEPVVQDSEPKEVPAVVNEKEVPAEPETQPPV
VAP27   --KLRVTYVAPPRPPSPVHEGSEEGSSPRASVSDNGHGSEFSFERFIVDNKAG------H
          *::*.*: .*   .. ::. :*....  .* ::.. .*..      :  *

Scs2    QVKKEEVPPVVQKTVPHENEKQTSNSTPAPQNQIKEAATVPAENESSSMGIFILVALLIL
VAP27   QENTSEARALITKLTEEKQSAIQLNNRLQRELDQLRRESKKSQSGGIPFMYVLLVGLIGL
        * :..*. .:: * . .::.    *.    : :  .  :  ::. . .:  .:**.*: *

Scs2    VLGWFYR--
VAP27   ILGYIMKRT
        :**:: :
```

F.

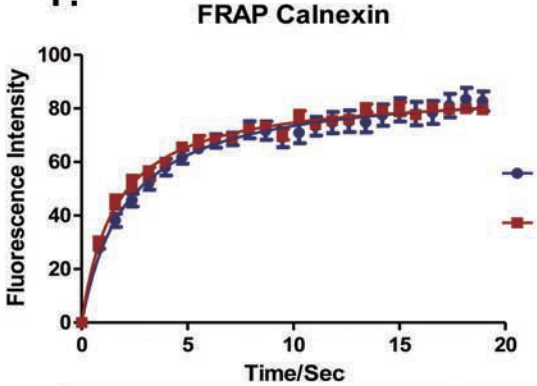

	Max Recovery (%)	Half Time (s)
CXN + Lat B (n=12)	86.65 ± 5.09	1.80 ± 0.44
CXN + Ory (n=12)	89.16 ± 7.35	2.12 ± 0.63

G.

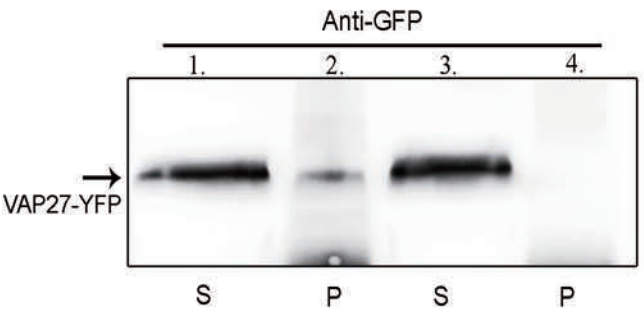

1. VAP27-RFP+ VAP27-YFP, Supernatant
2. VAP27-RFP+ VAP27-YFP, Pellet
3. VAP27-YFP, Supernatant
4. VAP27-YFP, Pellet

Figure S3. VAP27 is an ER membrane protein and also localises to PM/ER contact sites. Related to Figure 3.

(A) Time series of VAP27-YFP over 30 seconds. Each picture represents a time point from Movie S2 and is pseudo-coloured to represent the different time frames; red (0 seconds), green (15 seconds) and cyan (30 seconds). A merged picture indicates that the punctae are persistent (magenta) while the rest of the ER network remodels. **(B)** Expression of VAP27-GFP in Arabidopsis driven by its endogenous promoter. Static punctae at the ER/PM contact sites were observed, similar to those from transient expression studies. Notably, the size of VAP27 punctae varies from 0.25 to 1.5µm. **(C)** TEM images of Arabidopsis expressing VAP27-YFP (35S promoter). Close association between the ER and PM was also observed at the ultra-structural level. The size of ER/PM site 1 and 2 were measured and found to be about 0.5 and 1.0µm respectively, which is consistent with those observed using confocal microscopy. **(D)** Expression of yeast Scs2p-GFP with VAP27-YFP in plants. The two proteins co-localise at the ER network as well as at the ER/PM contact sites. **(E)** Alignment of VAP homologues in Arabidopsis (VAP27) and *Saccharomyces* (Scs2). Lysine 58, tyrosine 59 & 60 are conserved (highlighted in red) and these residues are involved in protein interactions through a FFAT motif in animals and yeast. The functional major sperm domain is highlighted in blue. **(F)** Fluorescence-recovery after photobleaching (FRAP) of calnexin-GFP (ER membrane protein, the transmembrane domain of calnexin fused to GFP) at ER cisternae with different drug treatments. Protein mobility on the ER membrane is not affected when cells were treated with either latruculin B (Rmax=86.7±5.1) or oryzalin (Rmax=89.2±7.4). **(G)** Immuno-precipitation of VAP27-RFP and VAP27-YFP using a RFP antibody. VAP27-YFP was found in the pellet fraction in the presence of VAP27-RFP (lane 1 and 2) indicating the protein is able to self-interact (scale bar = 5 µm for confocal; scale bar = 500 nm for TEM).

Figure S4

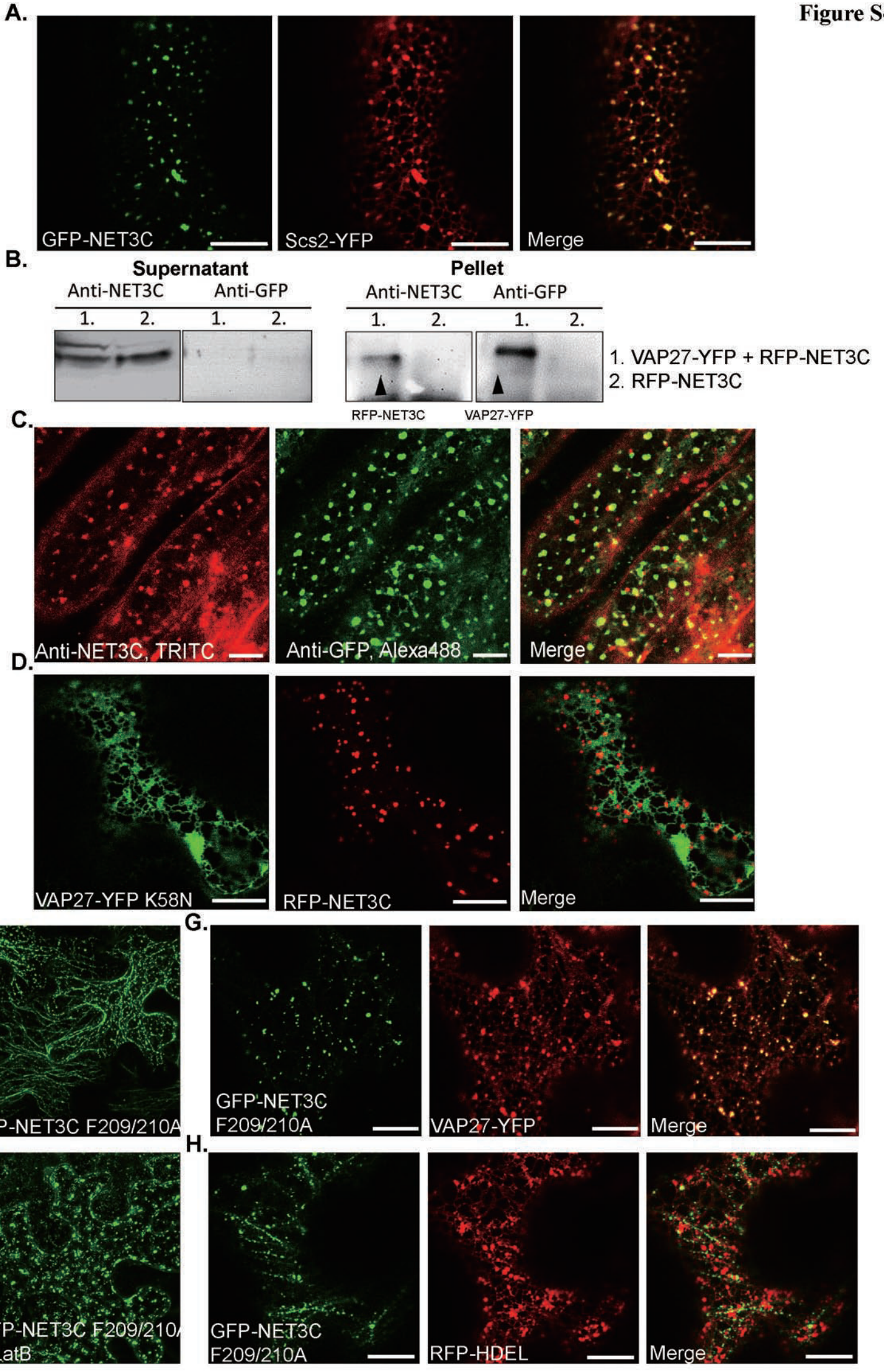
A.
GFP-NET3C
Scs2-YFP
Merge
B.
Supernatant
Pellet
Anti-NET3C
Anti-GFP
Anti-NET3C
Anti-GFP
1. 2. 1. 2.
1. 2. 1. 2.
1. VAP27-YFP + RFP-NET3C
2. RFP-NET3C
RFP-NET3C
VAP27-YFP
C.
Anti-NET3C, TRITC
Anti-GFP, Alexa488
Merge
D.
VAP27-YFP K58N
RFP-NET3C
Merge
E.
GFP-NET3C F209/210A
F.
GFP-NET3C F209/210A
+ LatB
G.
GFP-NET3C
F209/210A
VAP27-YFP
Merge
H.
GFP-NET3C
F209/210A
RFP-HDEL
Merge

Figure S4. VAP27 interacts with NET3C. Related to Figure 4.

(A) Similar to VAP27, Scs2-YFP also co-localised with GFP-NET3C at the ER/PM contact site. **(B)** Immuno-precipitation of RFP-NET3C and VAP27-YFP using GFP antibody. The Western blot was probed with either NET3C or GFP antibody. Note RFP-NET3C is found in the pellet fraction when co-expressed with VAP27-YFP (Sample 1), while the RFP-NET3C control (sample 2) is only found in the supernatant. **(C)** Immunofluorescence of NET3C in a stable Arabidopsis line expressing VAP27-YFP (35S promoter). Note the co-localisation of two proteins at punctae in the hypocotyl cells. **(D)** Site-directed mutagenesis in the major sperm domain. VAP27 K58N is still found at the ER network but fails to associate with the ER/PM contact site and NET3C. **(E**)Max projection of GFP-NET3C F209/210A in transient expressed cells. The mutant binds to F-actin producing the characteristic beads-on-string pattern. **(F)** GFP-NET3C F209/210A labeled filaments are sensitive to lactruculin B treatment (max projection). **(G)** GFP-NET3C F209/210A still interacts with VAP27 but the structure of VAP27 labeled ER/PM contact sites is affected. **(H)** Site-direct mutagenesis at the C-terminal tail of NET3C. NET3C F209/210A binds to F-actin but fails to associate with any membrane compartment. The ER network (Red) is distorted and fragmented in the presence of NET3C F209/210A mutant (Scale bar = 10 μm).

Supplemental Experimental Procedures

Plant material and transformations

Arabidopsis (Col-0) was grown on either ½ MS agar or compost in a growth chamber with 16hr light (22 °C) and 8hr darkness (18 °C). Stable Arabidopsis lines were transformed by floral-dipping as described in Zhang et al. [S1]. *Nicotiana benthamiana* was kept in a growth room with 16hr light (25°C) and 8hr darkness (18°C). Transient expression was performed by leaf infiltration according to Sparkes et al. [S2].

Molecular cloning

The cDNAs of NET3C and VAP27 were cloned from 10 day old Arabidopsis seedlings by RT-PCR (Invitrogen). Scs2 was cloned from total cDNA of *Saccharomyces cerevisiae.* The fluorescent protein fusions of NET3C and VAP27 were cloned into various binary vectors by Gateway reactions (Invitrogen). pMDC43 (N-terminal GFP), pMDC83 (C-terminal GFP), pH7WGR2 (N-terminal mRFP) and pCAMBIA1300-Cas-YFP (C-terminal YFP) were used. The VAP27 gene (genomic sequence including 2Kb upstream of ATG) cloned into pMDC107 for endogenous expression of GFP tagged VAP27. Domain deletion constructs were generated by over-lap PCR according to Heckman and Pease [S3]. Point mutation was performed according to the protocol provided with the site-direct mutagenesis kit (Agilent Technologies). The antigen fragment of NET3C was cloned into pGAT4 Gateway vector [S4] (with N-terminal HisTag) for *in-vitro* protein expression in *E.coli* (Rosetta 2, Novagen). Primers used in this study are listed in Supplementary Table S1.

Antibodies and immunofluorescence

Antigen peptide of NET3C (residue 120-161) was expressed and purified using nickel agarose beads (Qiagen). Polyclonal antibodies were raised in mice as described in Smertenko et al. [S5]. For the immunofluorescence study, root tips were fixed in 4% PFA in PIPES buffer (0.1M PIPES pH6.9, 1mM MgSO4, 2mM EGTA) for 90min followed by Driselase (2%) digestion for 7min. Samples were treated with 0.5% Triton for 5min and incubated in primary and secondary antibody for 3 hours or overnight at 4°C. In between each step, samples were washed with PBS buffer for three times. For double staining with GFPHDEL or FABD2GFP expressing cells, NET3C anti-serum and GFP

antibody (Abcam) was used at 1:500 dilutions, followed by secondary antibody incubation with TRITC-conjugated against mouse (Jackson ImmunoResearch) and Alexa488-conjugated against rabbit (Invitrogen). Samples were mounted with Vectashield prior to imaging.

Live cell imaging and FRET-FLIM

Transient transformed *N. benthamiana and N.tobaccum* were imaged two days after infiltration using laser scanning confocal microscopes (LSCM, Leica SP5 or Zeiss Meta510). Images were taken in multi-track mode with line switching when multi fluorescence was used. FRAP experiments and data analyses were performed as described in Wang et al. [S6]; a minimum number of 12 areas of interest were bleached from each individual cells. NET3C and VAP27 co-alignment on ER or cytoskeleton was analysed in 8 individual cells; an area of 100μm^2 from each cell was used. For drug treatment, leaf segments were incubated in 25 μM latrunculin B (40min) or 20 μM Oryzalin (30min) to depolymerise actin filaments or microtubules respectively.

FRET-FLIM experiments were carried out using a LeicaSP5 LSCM installed with fluorescence lifetime system (PicoQuant). The data acquisition and analysis were performed using SymPho Time software (PicoQuant). The lifetime of the GFP donor construct alone was measured as the negative control, whereas the GFP lifetime of GFP-RFP protein fusion was used as a positive control. All measurements were taken from whole field images expressing fluorescence protein at the similar level.

Transmission electron microscopy and immune-gold labeling

Arabidopsis tissue was fixed by high-pressure freezing with freeze substitution as described in Deeks et al. [S7]. NET3C anti-serum was used at 1:100 dilution and detected by 5nm gold-conjugated anti mouse antibody.

Co-immunoprecipitation assay and western blotting

Transformed *N. benthamiana* leaf transiently expressing proteins of interest were homogenised in protein extraction buffer (NaCl 150mM, Tris-HCl 50mM pH8.0, EDTA 5mM pH8.0, DTT 5mM, Triton X-100 1%, glycerol 10% and complete proteinase inhibiter). The extract was centrifuged at 13,000 rpm for 10min (4°C). GFP-antibody (Abcam) was added to the supernatant and incubated on ice for 2 hours before adding

protein A-coupled agarose beads (Sigma). The mixture was then incubated at 4°C for 1 hour with agitation and centrifuged at 13,000rpm for 1min. The pellet was washed three times with extraction buffer then boiled at 95°C in SDS buffer. Samples were loaded onto a 12.5% SDS-gel followed by electrophoresis and protein transfer. For detection, the membrane was incubated in 2xTBST buffer with 5% milk prior to primary antibody incubation (1:500-1000) at room temperature for 3 hours. After three washes in TBST buffer, the membrane was blotted in HRP-conjugated mouse secondary antibody (1:3000) and developed using an ECL reagent (GE heathcare).

Co-sedimentation assay

Protein extracts from *N. benthamiana* leaves transiently expressing VAP27-mRFP were used for the microtubule co-sedimentation assay. Polymerized microtubules were prepared as described in Smertanko et al. [S8]. Extraction buffer M (NaCl 100mM, Tris-HCl 50mM pH8.0, EGTA 5mM pH8.0, $MgCl_2$ 5mM and Triton X-100 0.5%) was used for the microtubule experiments. Before adding to the reaction tube, the extract was centrifuged at 13,000 rpm for 5min followed by 90,000 rpm for 15min (4°C) to remove cell debris or insoluble proteins. Protein and microtubules were mixed and incubated at room temperature for 15min. The mixture was then centrifuged at 70,000 rpm for 15min.

Protein extraction of NET3C from *N. benthamiana* leaves for F-actin co-sedimentation assays was performed similar to above, except extraction buffer A (KCl 20mM, Tris-HCl 5mM pH8.0, DDT 0.2mM, EGTA 2mM pH8.0, $MgSO_4$ 0.4mM and Triton X-100 0.1%) was used. Total protein containing GFP-NET3C was added to F-actin as described in Deeks et al. [S7]. For both experiments, supernatant and pellets (washed with extraction buffer) were mixed with SDS buffer then analyzed by western blotting.

Reverse genetics

The NET3B SALK T-DNA insertion line was ordered from NASC. Homozygosity was confirmed by PCR using gene specific primers, and T-DNA specific primer LBa1. There are no available insertion lines for NET3C. NET3C RNAi lines were ordered from AGRIKOLA. The RNAi insertion was confirmed using Agri primers as described in Hilson et al. [S9]. Total RNA was extracted from mature floral tissue (Qiagen). Frist-strand

cDNA was synthesized using Superscript III (Invitrogen) according to the manufacturer's protocol. RT-PCR was used to assess the presence of the full-length transcripts in *net3b* and *NET3C RNAi*. As a control, gene specific primers that amplify EF1a were used. Equal amounts of cDNA from either wild type or mutant Arabidopsis was used. All primers used in this study are listed in Supplementary table s1.

For phenotype studies, samples were viewed using a Zeiss Axioskop light microscope and an Olympus Research Stereo SZH10 microscope with appropriate magnification. Images were taken using Photometrics Coolsnap cf video camera and Openlab 3.1.1 software. Pollen grains were stained in DAPI solution (0.1M sodium phosphate butter, 1mM EDTA, 0.1% triton X-100, 0.4µg/ml DAPI) and studied using a Zeiss Meta510 confocal microscope with excitation at 405nm laser.

Chi-square analysis

In order to confirm that the association between NET3C punctae and the ER is not a coincidental event, chi-square tests were applied. The area of ER membrane and the ER-free area were measured, and the distribution of NET3C punctae scored as ER-associated or non-ER associated. The p value was calculated based on the real distribution of NET3C compared to the expected number from a random distribution. The same approach was used for the analysis of the NET3C/F-actin and NET3C/PM associations.

Supplemental table, list of primers used.

Name of Primer	Sequence (5'-3')
NET3C Constructs	
NET3C-F	gggg aca agt ttg tac aaa aaa gca ggc ttc ccg cca ATG GTT AGA GAA GAG GAG AAA TC
NET3C-RN	gggg acc ac ttt gta caa gaa agc tgg gtc CTA AAG GAC CTT GTT GCC ATC
NET3CΔNAB-F	gggg aca agt ttg tac aaa aaa gca ggc ttc ccg cca ATG TCT TCC GAC CAC TAT GGA TC
NET3C-Antigen-F	gggg aca agt ttg tac aaa aaa gca ggc ttc ccg cca ATG GAA GAC CCC CTT CAA GAT GA
NET3C-Antigen-R	gggg acc ac ttt gta caa gaa agc tgg gtc CTA GTC TAA GAG CTG TTT CCT CA
NET3C-K211A-RN	gggg acc ac ttt gta caa gaa agc tgg gtc CTA AAG GAC CGC GGC GCC ATC GCA C
NET3C-F209/210A-F	GCCACT AAACAAGGCC GCT GGGAAGC TGTTTTAC
NET3C-F209/210A-R	GTAAAACAGCTTCCCAGCGGCCTTGTTTAGTGGC
VAP Constructs	
VAP27-F	gggg aca agt ttg tac aaa aaa gca ggc ttc ccg cca ATG AGT AAC ATC GAT CTG
VAP27-RC	gggg acc ac ttt gta caa gaa agc tgg gtc TGTCCTCTTC
VAP27-RN	gggg acc ac ttt gta caa gaa agc tgg gtc TTA TGTCCTCTTC
VAP27 T59/60A-F	GCCTTTAAGGTTAAGGCGGCGAATCCGAAAAAG
VAP27 T59/60A-R	CTTTTTCGGATTCGCCGCCTTAACCTTAAAGGC
VAP27 K58N-F	GTTGCCTTTAAGGTTAACACGACGAATCCGAAAAAG
VAP27 K58N-R	CTTTTTCGGATTCGTCGTGTTAACCTTAAAGGCAAC
VAP27 Geno-F	gggg aca agt ttg tac aaa aaa gca ggc ttc ccg cca TTC ATA TCG GCT TCT TAC TCT
VAP27 Geno-R	gggg acc ac ttt gta caa gaa agc tgg gtc TGTCCTCTTCATAATGTATCCCA
Scs2p-F	gggg aca agt ttg tac aaa aaa gca ggc ttc ccg cca ATG TCT GCT GTT GAA ATT TCC
Scs2p-RC	gggg acc ac ttt gta caa gaa agc tgg gtc TCT GTA GAA CCA TCC TAA AAC C
Reverse Genetics and Genotyping	
NET3B-F	ATGGGTGAGACATCAAAATG
NET3B-R	CTA AAA CGA AAA CAT TAT GAG AAA ATA G
NET3C-F	ATG GTT AGA GAA GAG GAG AAA TC
NET3C-R	CTA AAG GAC CTT GTT GCC ATC
EF1a-F	CCCATTTGTGCCCATCTCT
EF1a-R	CACCGTTCCAATACCACCAA
Agri51	CAA CCA CGT CTT CAA AGC AA
Agri56	CTG GGG TAC CGA ATT CCT C
Agri64	CTT GCG CTG CAG TTA TCA TC
Agri69	AGG CGT CTC GCA TAT CTC AT

Supplemental References

S1. Zhang, X., Henriques, R., Lin, S.S., Niu, Q.W., and Chua, N.H. (2006). Agrobacterium-mediated transformation of Arabidopsis thaliana using the floral dip method. Nature protocols *1*, 641-646.

S2. Sparkes, I.A., Runions, J., Kearns, A., and Hawes, C. (2006). Rapid, transient expression of fluorescent fusion proteins in tobacco plants and generation of stably transformed plants. Nature protocols *1*, 2019-2025.

S3. Heckman, K.L., and Pease, L.R. (2007). Gene splicing and mutagenesis by PCR-driven overlap extension. Nature protocols *2*, 924-932.

S4. Deeks, M.J., Fendrych, M., Smertenko, A., Bell, K.S., Oparka, K., Cvrckova, F., Zarsky, V., and Hussey, P.J. (2010). The plant formin AtFH4 interacts with both actin and microtubules, and contains a newly identified microtubule-binding domain. J Cell Sci *123*, 1209-1215.

S5. Smertenko, A.P., Kaloriti, D., Chang, H.Y., Fiserova, J., Opatrny, Z., and Hussey, P.J. (2008). The C-terminal variable region specifies the dynamic properties of Arabidopsis microtubule-associated protein MAP65 isotypes. Plant Cell *20*, 3346-3358.

S6. Wang, P., Hummel, E., Osterrieder, A., Meyer, A.J., Frigerio, L., Sparkes, I., and Hawes, C. (2011). KMS1 and KMS2, two plant endoplasmic reticulum proteins involved in the early secretory pathway. Plant J *66*, 613-628.

S7. Deeks, M.J., Calcutt, J.R., Ingle, E.K., Hawkins, T.J., Chapman, S., Richardson, A.C., Mentlak, D.A., Dixon, M.R., Cartwright, F., Smertenko, A.P., et al. (2012). A superfamily of actin-binding proteins at the actin-membrane nexus of higher plants. Curr Biol *22*, 1595-1600.

S8. Smertenko, A.P., Chang, H.Y., Wagner, V., Kaloriti, D., Fenyk, S., Sonobe, S., Lloyd, C., Hauser, M.T., and Hussey, P.J. (2004). The Arabidopsis microtubule-associated protein AtMAP65-1: molecular analysis of its microtubule bundling activity. Plant Cell *16*, 2035-2047.

S9. Hilson, P., Allemeersch, J., Altmann, T., Aubourg, S., Avon, A., Beynon, J., Bhalerao, R.P., Bitton, F., Caboche, M., Cannoot, B., et al. (2004). Versatile gene-specific sequence tags for Arabidopsis functional genomics: transcript profiling and reverse genetics applications. Genome Res *14*, 2176-2189.